

Electronic Thesis and Dissertation Repository

9-29-2021 12:00 PM

Development of 3D Bioartificial Human Tissue Models of Periprosthetic Shoulder Joint Infection

Tony B. Huang, *The University of Western Ontario*

Supervisor: O'Gorman, David B., *The University of Western Ontario*

Co-Supervisor: Burton, Jeremy P., *Lawson Health Research Institute*

A thesis submitted in partial fulfillment of the requirements for the Master of Science degree in Biochemistry

© Tony B. Huang 2021

Follow this and additional works at: <https://ir.lib.uwo.ca/etd>



Part of the [Biochemistry Commons](#)

Recommended Citation

Huang, Tony B., "Development of 3D Bioartificial Human Tissue Models of Periprosthetic Shoulder Joint Infection" (2021). *Electronic Thesis and Dissertation Repository*. 8172.

<https://ir.lib.uwo.ca/etd/8172>

This Dissertation/Thesis is brought to you for free and open access by Scholarship@Western. It has been accepted for inclusion in Electronic Thesis and Dissertation Repository by an authorized administrator of Scholarship@Western. For more information, please contact wlsadmin@uwo.ca.

Abstract

Periprosthetic joint infection (PJI) is a devastating and costly post-surgical complication that is not well understood due to the scarcity of physiologically representative experimental models. This thesis outlines the development of two 3D bioartificial human tissue models designed to study the cellular and biochemical interactions between primary fibroblasts from the shoulder capsule (SC) and infectious microorganisms. Using the Fibroblast-Bacteria Co-culture in 3D Collagen model, we demonstrated a global gene repression of metabolic and homeostatic processes in SC fibroblasts following 48 hours of co-culture with *Cutibacterium acnes* – the most common microbial cause of PJI in the shoulder. These cellular changes coincided with an increase in pro-inflammatory signaling. The Shoulder-Joint Implant Mimetic (S-JIM) model generated a range of oxygen levels (< 0.3% to 21% O₂) that accurately represents the different microenvironments present across connective tissue layers in a shoulder joint. Electron microscopy images confirmed that the hypoxic conditions generated in the core of the S-JIM supported the anaerobic proliferation of *C. acnes*, but this microbial expansion resulted in the death of adjacent SC fibroblasts after 96 hours of co-culture. Using the S-JIM, we demonstrated the bactericidal effectiveness of direct vancomycin prophylaxis against *C. acnes* and confirmed the possibility of differentiating between healthy host tissues and *C. acnes*-infected tissues using mass spectrometry.

Key Words

Tissue engineering, periprosthetic joint infection, *Cutibacterium acnes*, 3D bioartificial tissue model, infection prophylaxis, shoulder joint capsule

Summary for Lay Audience Abstract

Bacterial infection may sometimes develop on the surface of an implant after joint replacement surgery. These complications can have devastating consequences on a patient's physical and mental wellbeing, resulting in a heavy healthcare burden. The shoulder joint is particularly susceptible to infection by *Cutibacterium acnes* – a species of skin bacteria that may begin to proliferate in the low-oxygen environment close to the implant. The details on how a *C. acnes* infection damages the shoulder joint is not well understood at present due to limitations in our current models of joint infection.

In this thesis, we outline the development of two novel laboratory models of joint infection that were created using human shoulder cells. Our first model, the Fibroblast-Bacteria Co-culture in 3D Collagen, was designed to assess for changes in the expression of genes in shoulder cells following an artificially induced *C. acnes* infection. We observed an overall decrease in the expression of genes that regulate cell stability and growth, but an increase in the expression of genes that signal for an inflammatory response. These changes in the shoulder cells are consistent with the physiological responses that would be present following joint infection in a patient.

Our second model, the Shoulder-Joint Implant Mimetic (S-JIM) was designed to replicate the low-oxygen conditions that would be generated near the implant surface by the many layers of dense shoulder tissue surrounding the implant. Microscope images confirmed that the low-oxygen conditions generated in the core of the S-JIM supported the proliferation of *C. acnes*, and that this continued microbial growth killed adjacent shoulder cells after 96 hours. Using the S-JIM, we also demonstrated that the preemptive application of vancomycin powder (a first-choice antibiotic for clearing orthopedic infections) was successful at completely eradicating *C. acnes* cells from the model and prevented the development of infection. Finally, we provided proof-of-concept for the use of mass spectrometry – a method of detecting specific molecular markers – to differentiate between healthy shoulder tissues and tissues infected with *C. acnes*.

Co-Authorship Statement

All experiments and subsequent data analyses described in this thesis were performed by Tony Huang unless otherwise stated. All figures, tables, and videos shown in this thesis were produced by Tony Huang with the following exceptions:

Figure 1.1 was generated from unpublished data by Athir Jisrawi (O’Gorman laboratory) prior to the commencement of this thesis.

Figure 1.2 was generated from an image provided by Joan Miquel i Noguera from St. Joseph’s Hospital.

Figure 4.7 was generated from data that was derived in collaboration with Joan Miquel i Noguera.

Figure 4.8 was generated by Michael Woolman from the University of Toronto.

Table 1.1 was generated from published data by Carreau *et al.*, as cited below.

Acknowledgements

I would like to express my sincerest gratitude to my research supervisor, Dr. David O’Gorman, for his time, patience, and amazing mentorship. He has provided me with numerous opportunities, both in and outside the lab, to grow as an independent thinker. Under Dr. O’Gorman’s guidance, I have strengthened my presentation skills, learned the importance of scientific networking, and most importantly, developed the confidence to design my own experiments. I am tremendously grateful not only for his teachings, but also for the trust he placed in me to eventually take charge of my project, despite my numerous initial mistakes. His mentorship was critical to my successes, and I cannot thank him enough for providing me with this amazing research experience.

I would also like to acknowledge my graduate advisory committee members, Dr. Jeremy Burton and Dr. David Haniford, for their continued support and guidance. Their feedback throughout my thesis was vital towards my growth as a scientific thinker. Furthermore, I would like to recognize the important contributions of Lynn Keenlside in helping to create several of the components and tools used in the S-JIM models. I am furthermore grateful towards our collaborators Michael Woolman and Dr. Arash Zarrine-Afsar for lending their expertise in mass spectrometry for our project, Dr. John Miquel i Noguera for his help in conducting the vancomycin experiments, and Karen Nygard for providing me with microscopy assistance.

Lastly, I’d like to thank Ana Pena Diaz, Johnny Luo, and all of the members of the O’Gorman lab for sharing this experience with me. Ana and Johnny have both sacrificed much of their personal time in helping me develop the research techniques and mindset to succeed as an independent learner, for which I am tremendously grateful. It is undeniable that their support and encouragement made my research experience all the more enjoyable, and I am honored to have been able to work alongside such an amazing and reliable research team.

Table of Contents

Abstract	i
Key Words	i
Summary for Lay Audience Abstract	ii
Co-Authorship Statement.....	iii
Acknowledgements.....	iv
List of Tables	ix
List of Figures	x
List of Abbreviations	xii
Chapter 1	1
1 LITERATURE REVIEW.....	1
1.1 Periprosthetic Joint Infection (PJI)	1
1.1.1 Overview.....	1
1.1.2 Healthcare Burden	5
1.1.3 PJI Management.....	5
1.1.4 Symptoms and Risk Factors.....	6
1.1.5 PJI in the Shoulder	7
1.2 <i>Cutibacterium acnes</i>	7
1.2.1 Microbiology.....	7
1.2.2 Opportunistic Pathogen.....	8
1.2.3 Biofilm Formation	11
1.2.4 Diagnostic Challenges	12
1.3 Current models of PJI	13
1.3.1 Overview.....	13
1.3.2 Animal Models.....	14

1.3.3	<i>Ex vivo</i> Models.....	15
1.3.4	<i>In vitro</i> Models.....	15
1.4	Objectives and Rationale	16
Chapter 2	21
2	MATERIALS AND METHODS.....	21
2.1	Sample Collection.....	21
2.1.1	Primary Human Fibroblasts	21
2.1.2	<i>Cutibacterium acnes</i>	21
2.2	Fibroblast-bacteria Co-culture in 3D Collagen Setup.....	22
2.3	Shoulder-Joint Implant Mimetic Model Setup	22
2.4	Desorption Electrospray Ionization Mass Spectrometry	23
2.5	Quantification of Gene Expression.....	24
2.5.1	RNA Extraction from FPCL Samples.....	24
2.5.2	RNA Extraction from S-JIM Samples	24
2.5.3	cDNA Synthesis.....	25
2.5.4	Real Time PCR	25
2.5.5	Statistical Analysis.....	25
2.5.6	RNA Sequencing	25
2.6	S-JIM Cell Imaging.....	26
2.6.1	EF5 Hypoxia Labelling.....	26
2.6.2	Live-Dead Mammalian Cell Labeling	26
2.6.3	Scanning Electron Microscopy	27
Chapter 3	28
3	FIBROBLAST-BACTERIA CO-CULTURE IN 3D COLLAGEN (FBCC)	28
3.1	Validation of Model and Suitable Housekeeping Gene in SC Fibroblasts Following Co-culture with <i>C. acnes</i>	28

3.2	Impact of <i>C. acnes</i> on SC Fibroblasts Gene Expression	32
3.3	Net Changes in SC Fibroblast Gene Expression in Response to a <i>C. acnes</i> Infection	37
	Chapter 4.....	40
4	Shoulder-Joint Implant Mimetic (S-JIM)	40
4.1	Model Development and Optimization.....	40
4.2	Custom S-JIM Assembly Tools	41
4.3	Generating an Oxygen Accessibility Gradient Across S-JIM Strip Layers.....	44
4.4	<i>C. acnes</i> Induces SC Fibroblast Cell Death	47
4.5	<i>C. acnes</i> Grows on Titanium Alloy Surfaces in an S-JIM but Does Not Form a Biofilm	49
4.6	Identifying Putative Biomarkers of <i>C. acnes</i> PJI.....	52
4.7	Applications of the Shoulder-Joint Implant Mimetic	54
4.7.1	Overview.....	54
4.7.2	Validation of Vancomycin Prophylaxis in <i>C. acnes</i> PJI.....	54
4.7.3	Detecting <i>C. acnes</i> PJI by Desorption Electrospray Ionization Mass Spectrometry	59
	Chapter 5.....	61
5	Shoulder-Joint Implant Mimetic (S-JIM)	61
5.1	<i>C. acnes</i> Induces a Pro-Inflammatory Response in SC Fibroblasts.....	61
5.2	Limitations of the FBCC Model	63
5.3	Potential Improvements to the S-JIM Model.....	64
5.4	SC Cell Death in the Presence of <i>C. acnes</i>	65
5.5	Bactericidal Efficiency of Vancomycin Against <i>C. acnes</i> in the S-JIM.....	66
5.6	Explanations for the Lack of Biofilm Formation in the S-JIM.....	67
5.7	Prospective Real-Time Detection of <i>C. acnes</i> PJIs Using Mass Spectrometry	71

5.8 Conclusion	72
References	73
Supplementary Information	84

List of Tables

Table 1.1 Normal oxygen percentage in the microenvironment of various tissues.....	4
Table 4.1. Modifications to Cell Culture Parameters and Model Setup from the TRACER to S-JIM System.....	42
Table 4.2. <i>C. acnes</i> survival following vancomycin application in the S-JIM.....	58
Table S1. SC Fibroblast Cellular Pathways with Enhanced Gene Expression Following Co-culture with <i>C. acnes</i> in the FBCC Model.....	85

List of Figures

Figure 1.1. Proliferation of Primary Tenocytes in 3D Collagen.....	3
Figure 1.2. The shoulder joint capsule during arthroplasty.....	10
Figure 1.3. Fibroblast-bacteria Co-culture in 3D Collagen (FBCC) Model.....	17
Figure 1.4. Shoulder-Joint Implant Mimetic (S-JIM) Model.....	19
Figure 3.1. <i>In vitro</i> Growth Curve of <i>C. acnes</i> CA01.....	29
Figure 3.2. Evaluating suitable SC fibroblast housekeeping genes.....	31
Figure 3.3. <i>C. acnes</i> elicits an <i>in vitro</i> inflammatory response in SC fibroblasts.....	33
Figure 3.4. Expression of toll-like receptor genes are suppressed in SC fibroblasts following co-culture with <i>C. acnes</i>	35
Figure 3.5. Expression of extracellular matrix genes are suppressed in SC fibroblasts following co-culture with <i>C. acnes</i>	36
Figure 3.6. Heatmap of differentially expressed mRNA in SC fibroblasts cultured in the FBCC model with or without <i>C. acnes</i>	39
Figure 4.1 Custom-designed cell culture tools for S-JIM setup.....	43
Figure 4.2. Gradient of oxygen levels in the S-JIM.....	46
Figure 4.3. <i>C. acnes</i> Induces SC Fibroblast Cell Death.....	48
Figure 4.4. <i>C. acnes</i> Growth on Ti6Al4V Titanium Alloy Foils in the S-JIM.....	50
Figure 4.5. <i>C. acnes</i> aggregates on the surface of Ti6Al4V titanium-alloy foils.....	51
Figure 4.6. Putative SC Fibroblast Biomarker Gene Expression Changes in Response to <i>C. acnes</i> in the S-JIM.....	53

Figure 4.7. SC fibroblasts do not alter vancomycin degradation rate.....	57
Figure 4.8. Detection of Ions Specific to <i>C. acnes</i> and SC fibroblast in S-JIM strips.....	60
Figure 5.1. 3D Microbial Clustering During Biofilm Initiation.....	70
Figure S1. Differential gene expression of the (A) TNF and (B) IL-17 signaling pathways in SC fibroblasts in response to <i>C. acnes</i>	87

List of Abbreviations

16S rRNA	16 Subunit Ribosomal Ribonucleic Acid
ACTB	Beta-actin
AI-2	Autoinducer 2
ANGPTL4	Angiopoietin-like 4
ARC	Adult Rotator Cuff
ATCC	American Type Culture Collection
BHI	Brain Heart Infusion
CA01	<i>C. acnes</i> Strain 01
CAMP	Christie-Atkins-Munch-Peterson
CCL2	C-C Motif Chemokine Ligand 2
CD8	Cluster of Differentiation 8
CFU	Colony Forming Unit
CMM	Counts Per Million
COL1A1	Collagen Type I Alpha 1 Chain
COL3A1	Collagen Type III Alpha 1 Chain
CPA4	Carboxypeptidase A4
Ct	Cycle Threshold
Cy3	Cyanine 3
DAPI	4',6-diamidino-2-phenylindole
DDIT3	DNA Damage Inducible Transcript 3
DESI-MS	Desorption Electrospray Ionization Mass Spectrometry
DMEM	Dulbecco Modified Eagle Medium
DMEM-soy	Dulbecco Modified Eagle Medium + 0.4% soytone
ECM	Extracellular Matrix
EPS	Extracellular Polymeric Substances
FBCC	Fibroblast-bacteria Co-culture in 3D Collagen
FPCL	Fibroblast Populated Collagen Lattice
GAPDH	Glyceraldehyde 3-phosphate dehydrogenase
GSA	Gene Specific Analysis

HAS3	Hyaluronan Synthase 3
hg38	Human Reference Genome 38
HIF1A	Hypoxia Inducible Factor 1A
iKnife	Intelligent Knife
IL-6	Interleukin-6
IL-10	Interleukin-10
IL-17	Interleukin-17
m/z	Atomic Mass/Atomic Number
MIC	Minimal Inhibitory Concentration
mRNA	Messenger RNA
NDF4	Neuron Derived Neurotrophic Factor 4
NRC	Normal Rotator Cuff
PBS	Phosphate-buffered Saline
PCR	Polymerase Chain Reaction
PJI	Periprosthetic Joint Infection
PTGS2	Prostaglandin-Endoperoxide Synthase 2
qPCR	Qualitative Polymerase Chain Reaction
RCD	Rotator Cuff Disease
REIMS	Rapid Electrospray Ionization Mass Spectrometry
RNA-seq	Ribonucleic Acid Sequencing
RPLP0	Ribosomal Protein Lateral Stalk Subunit P0
SC	Shoulder Capsule
SEM	Scanning electron microscopy
S-JIM	Shoulder-Joint Implant Mimetic
STAR	Spliced Transcript Alignment to a Reference
STAT3	(Signal Transducer And Activator Of Transcription 3)
STC1	Stanniocalcin-1
Ti6Al4V	1-Titanium 6-Aluminum 4-Vanadium
TLR	Toll-like Receptor
TNF	Tumor Necrosis Factor
TRACER	Tissue Roll for Analysis of Cellular Environment and Response

Chapter 1

1 LITERATURE REVIEW

1.1 Periprosthetic Joint Infection (PJI)

1.1.1 Overview

Infection occurs when microorganisms invade a host organism's tissues and disturb the native cellular environment by secreting disease-causing toxins and/or by usurping local cellular resources for their own rapid proliferation. These microbial activities can destabilize the host organism's native microbiota and disrupt essential biological processes, such as cell signaling and tissue regeneration.

In humans, infection develops infrequently in internal organs and tissues as they are shielded from exogenous pathogens by thick layers of skin, fat, and muscle. However, in the event of an injury, internal organs and tissues may be exposed to airborne contaminants and microorganisms from other parts of the body, allowing opportunistic pathogens to colonize these previously inaccessible regions.

Surgery is a special type of artificial injury that may inadvertently enable microbial invasion of human tissues. For example, in joint replacement surgery, the process of reconstructing a functional joint can expose adjacent connective tissues to bacteria from the surrounding dermis. Although precautions are generally taken to avoid contact between the joint cavity and dermal layers, technical errors during the operation can result in cross-contamination of tissues. In most US hospitals, joint infection occurs in about 0.5% to 2% of knee replacements, 0.5% to 1.0% of hip replacements, and less than 1% of shoulder replacements.¹⁻³

The human joint cavity provides an advantageous microenvironment for the proliferation of anaerobic bacteria. In the rotator cuff (i.e., the muscles and tendons that support the shoulder joint), primary tenocytes grow optimally under low-oxygen (2% O₂), but they stop growing and differentiate toward a tissue repair-associated myofibroblast phenotype when cultured under atmospheric oxygen levels (21% O₂) **Figure 1.1**. The adaptation of

these cells to grow under low-oxygen conditions *in vitro* is reflective of low-oxygen conditions in the joint. Compared to the oxygen availability in most other human tissues⁴, the shoulder joint cavity is relatively hypoxic (**Table 1**).

The microenvironment within a post-surgical joint cavity is hypothesized to be even more hypoxic than in normal joints, as prosthetic joints do not have the vasculature of a normal joint. Instead, the addition of an artificial implant induces the foreign body reaction – a non-specific immune response whereby the implant becomes encapsulated in a dense layer of fibrotic connective tissue.⁵ This scar-like tissue has poor vascularity, which when combined with the avascular nature of the metal implant, limits the rate of oxygen diffusion into the joint cavity. This in turn generates an abnormally hypoxic microenvironment that can provide anaerobic pathogens with a fitness advantage and promote the development of periprosthetic joint infection (PJI).

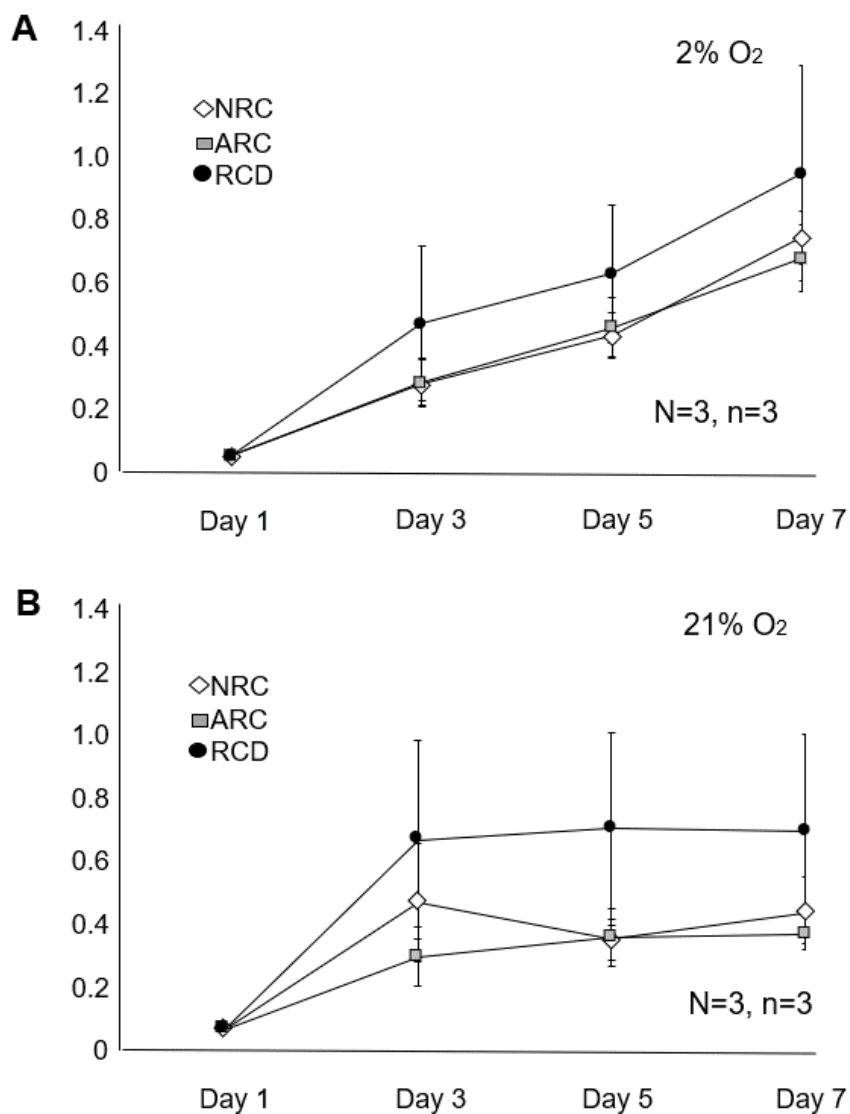


Figure 1.1. Proliferation of Primary Tenocytes in 3D Collagen.

Growth of primary tenocytes derived from the supraspinatus and subscapularis tendons from normal rotator cuff (NRC, patient age 18 - 35 years), adult rotator cuff (ARC, patient age 36 - 65 years) and torn rotator cuff (RCD, patient age 60 -75 years). Under 21% O₂, tenocytes displayed rapid growth rates initially that consistently plateaued after 3 days and cells developed a myofibroblast-like morphology with multiple cellular processes. Under 2% O₂, the cells grew more slowly and constantly while maintaining a typical rounded tenocyte morphology. Unpublished data by Athir Jisrawi (O’Gorman laboratory) generated prior to the commencement of this thesis.

Table 1.1 Normal oxygen percentage in the microenvironment of various tissues.⁴

Human tissue	% O₂
Bone marrow	6.4 ± 0.6
Brain	4.4 ± 0.3
Lungs	5.6
Skin (sub-papillary plexus)	4.6 ± 1.1
Skin (dermal papillae)	3.2 ± 0.8
Skin (superficial region)	1.1 ± 0.4
Intestinal tissue	7.6 ± 0.3
Liver	5.4 ± 0.7
Kidney	9.5 ± 2.6
Muscle	3.8 ± 0.2
Air	21.1

1.1.2 Healthcare Burden

PJI results from a failure to maintain aseptic conditions during arthroplasty (i.e. the surgical reconstruction or replacement of a joint) and remains one of the leading causes of revision surgery worldwide.⁶ Infection can occur following the replacement of any joint, including the hip, knee, shoulder, elbow, wrist, ankle, temporomandibular, metacarpophalangeal, and interphalangeal joints. However, the vast majority of PJI cases involve the hip, knee, and shoulder joints as these surgeries are more routinely performed.⁷

PJI places a heavy burden on healthcare spending. While only 1 to 3% of arthroplasty patients develop PJIs, the costs associated with managing infection are staggering.⁸ Multiple revision surgeries may be required to control a persistent infection. For example, revision of a knee arthroplasty may cost 3 to 4 times as much as the initial operation due to a higher number of operations and examinations, and longer operative times.⁹ Moreover, the failure rate for revision surgery can be as high as 33%.¹⁰ In the US, the estimated annual cost of treating PJI in 2020 is \$1.62 billion.¹¹

1.1.3 PJI Management

Periprosthetic joint infection generally develops as a result of surgical contamination, but an estimated 20% to 35% of cases may also arise from hematogenous spread.¹² The latter situation arises when a patient with a pre-existing prosthetic joint encounters an injury that allows bacteria from the wound to enter the circulation and eventually permeate the periprosthetic tissues. In both cases, routine treatment of PJI involves the surgical removal of the implant, followed by debridement and irrigation of periprosthetic tissues.¹³ Once new implant parts are reintroduced, patients are typically placed on long-term antibiotic therapy (~12 weeks), applied intravenously for the first two weeks and orally afterwards.¹⁴ The type and dosage of antibiotic used depends on the microbial source of infection, which is detected by collecting and culturing of intraoperative biopsy samples.¹⁴ In the case that infection cannot be controlled, the joint may need be amputated or permanently immobilized.¹⁵

PJI presents a clinical challenge as infection may persist after several revision surgeries, and patients who undergo repeated operations can develop permanent complications. Prolonged suppressive antibiotic therapy (either oral or intravenous) provides an alternative to further surgery. However, intraoperative antibiotics may disrupt the joint microbiota and oral antibiotics may disrupt the gut microbiota. Furthermore, both routes of antibiotic delivery risk promoting microbial resistance, and some patients may develop adverse drug reactions.¹⁶

The antibiotic vancomycin is a popular prophylaxis to orthopedic infections. In spinal fusion and shoulder replacement surgery, vancomycin powder is typically applied directly into the surgical site.^{17,18} However, the effectiveness of vancomycin in preventing PJIs is currently unclear, as large numbers of patient samples are required to conduct high-quality studies such as randomized controlled trials due to the low incidence of PJI in most hospitals. However, there are two potential problems with its prophylactic application. First, similar to prolonged suppressive antibiotic therapy, the use of vancomycin may promote microbial resistance. Second, a high serum concentration of vancomycin can increase the risk of renal function deterioration.¹⁹

1.1.4 Symptoms and Risk Factors

Common reported symptoms of PJI include non-specific pain, joint effusion or drainage, erythema, and fever.²⁰ PJI can also lead to serious clinical consequences such as tissue necrosis and implant loosening.²¹ General risk factors include tobacco abuse, obesity, rheumatoid arthritis, tumor growth, immunosuppression, and diabetes mellitus. A history of prior surgery at the site of operation and the duration of surgery itself can also increase the risk of PJI.²² PJI can be classified as either acute (<4 weeks after surgery and <3 weeks of symptoms) or chronic (≥ 4 weeks after surgery and ≥ 3 weeks of symptoms), depending on the onset and duration of symptoms.⁷ PJIs caused by surgical contamination typically present symptoms within the first month, whereas PJIs arising from hemorrhagic spread may occur at any point after the initial operation.²³

1.1.5 PJI in the Shoulder

The shoulder joint is one of the most common sites of arthroplasty. In the US, 53,000 total shoulder arthroplasties are performed annually.²⁴ *Cutibacterium acnes* is responsible for ~60% of all post-surgical cases of PJI in the shoulder, making it the most common microbial cause of infection in this region.²⁵ This contrasts with PJI in the knee and hip, whereby *Staphylococcus aureus* is the most common microbial pathogen.²⁶

1.2 *Cutibacterium acnes*

1.2.1 Microbiology

Cutibacterium acnes is a gram-positive, nonsporulating bacillus that resides naturally within the pilosebaceous follicles of human skin.^{27,28} As one of the most common commensal microorganisms of human skin, *C. acnes* represents up to 90% of the microbiota in some regions of the reticular dermis, such as the face, back, upper chest, and shoulder.^{29–32} *Cutibacterium acnes* thrives in this lipid-rich microenvironment by using its unique set of enzymes to metabolize sebum constituents into simple fats and carbohydrates. For example, *C. acnes* expresses two secretory lipases that degrade triglycerides, a sialidase that cleaves sialoglycoconjugates into sialic acid, and two putative endoglycoceramidases that are thought to break down oligosaccharides and glycosphingolipids.³³

The metabolic activity of *C. acnes* confers a protective function for the skin. By metabolizing sebum, *C. acnes* generates large quantities of the byproduct propionic acid, as well as other short chain fatty acids that help to maintain a low skin pH. These acidic conditions exclude microbial pathogens such as *Staphylococcus* and *Streptococcus* species from colonizing the skin.^{33,34}

The ability of *C. acnes* to produce propionic acid has resulted in its previous misclassification under the genus *Propionibacteria*. In 2016, a reclassification effort was undertaken to differentiate the environmental species found in dairy products and cattle rumen from the cutaneous species that have evolved to live in human skin. Whole-

genome analyses of strains belonging to the *Propionibacteriaceae* family identified specific lipase-encoding genes for degrading sebum lipids in the cutaneous bacteria, while several *Propionibacteriaceae* genes appeared to be lost. Substantial discrepancies were also found in the 16S rRNA gene sequence between the two bacterial groups, implying early divergent evolution. Because of these phylogenetic differences, the cutaneous bacteria previously recognized as *Propionibacterium* species were reclassified under the new genus *Cutibacterium*.³⁵

Cutibacterium acnes is a robust microorganism. While officially classified as an aerotolerant anaerobe, cutaneous *C. acnes* strains have been isolated by primary aerobic culture in as high as 28% of test subjects.³⁶ This implies that a substantial number of *C. acnes* strains possess both aerobic and anaerobic modes of growth. Genomic and transcriptomic analyses also support this notion. For example, Brzuszkiewicz *et al.* recorded the presence and gene expression of two respiratory endoxidases in *C. acnes*.³⁷ The trigger(s) that activate or deactivate each mode of growth are not well understood, but the ability of *C. acnes* to react to changing oxygen levels affords the bacterium increased survivability compared to strict anaerobes.

Cutibacterium acnes is a relatively slow-growing microorganism with an average doubling rate of 5 to 12 hours under anaerobic cell culture conditions; this doubling rate can vary dramatically depending on the strain phylotype and culture media selection.^{38–40} In its planktonic form, *C. acnes* divides by binary fission and has a rod-like morphology that lacks pili-like appendices on its cell wall.⁴¹

1.2.2 Opportunistic Pathogen

C. acnes contributes to a variety of human-related diseases, including acne vulgaris, sarcoidosis, aortic aneurysms, and several types of implant-associated infections.⁴² This has led researchers to view *C. acnes* not just as a skin commensal, but also as a potential opportunistic pathogen, particularly in the context of orthopedic infections. Recent microbiota analyses of the shoulder joint support this notion. When the bacterial microbiota of patient rotator cuff and skin samples were compared, ribosomal RNA (rRNA) gene sequences specific to *Cutibacterium* species were absent in the joint but

present in the skin, implying that *C. acnes*-associated PJI is a result of dermal contamination during surgery.⁴³ **Figure 1.2** illustrates the relative proximity of the different tissues exposed to the shoulder joint cavity during arthroplasty.

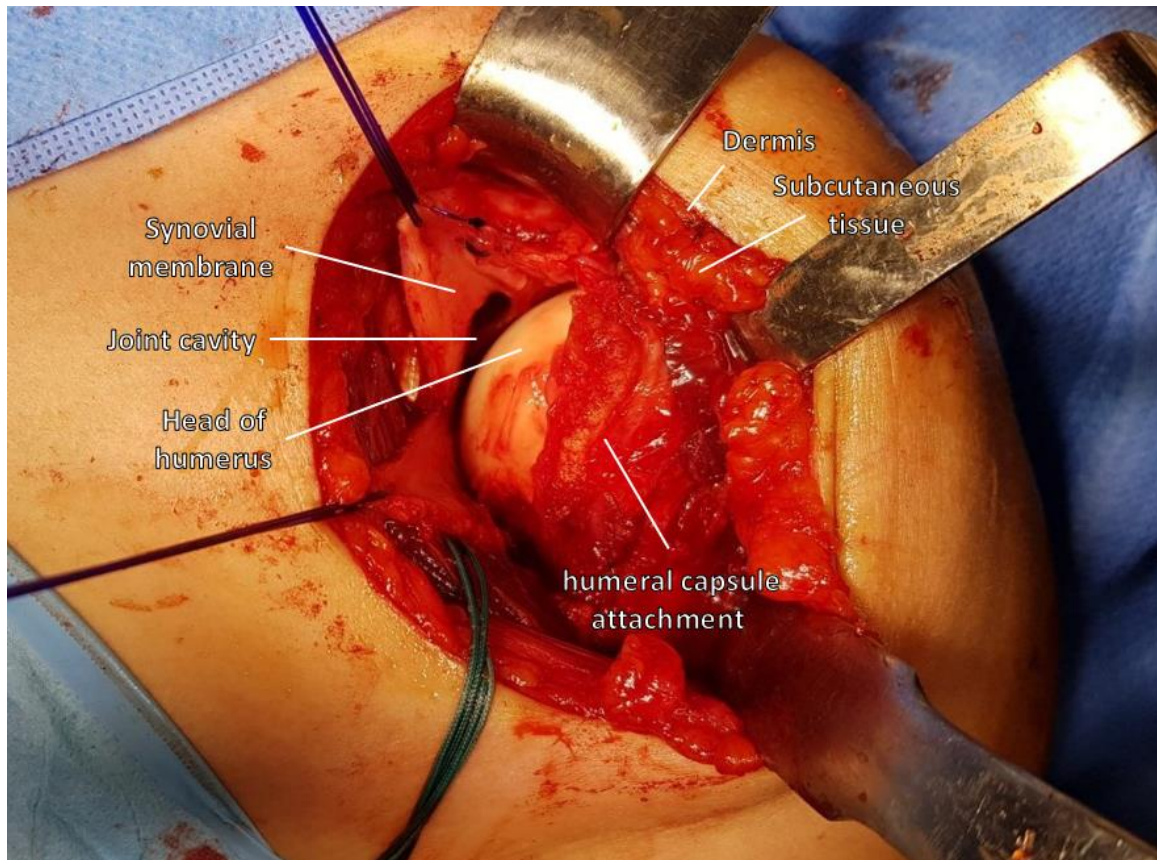


Figure 1.2. The shoulder joint capsule during arthroplasty.

Cutibacterium acnes colonizes the sebum-rich regions of subcutaneous tissues. Routine preoperative sterilization procedures can decontaminate skin surfaces on the shoulder, but they do not impact surgically exposed subcutaneous tissues.⁴⁴ In the process of replacing the humeral head, any tools that inadvertently graze the subcutaneous tissues risk introducing *C. acnes* into the joint cavity. Once the synovial membrane is re-ligated, the joint cavity eventually becomes hypoxic, which favors *C. acnes* proliferation. Image was derived from St. Joseph's Hospital, London, Canada.

1.2.3 Biofilm Formation

Microbial biofilms are complex communities of microorganisms that are attached to a surface and encapsulated within a matrix of extracellular polymeric substances.⁴⁵ Biofilm formation occurs in four stages: cell adherence, cellular aggregation, biofilm maturation, and cellular detachment. Initially, adhesion proteins or appendices on microbial cell walls form weak, transient interactions with the surface of an implant. Once adhered, cells begin to divide rapidly, forming aggregates of microcolonies. Once a critical microbial density is reached, cells slow their proliferation and begin to secrete autoinducers that transmit quorum signals to alter global gene expression. This causes the bacteria to secrete a meshwork of extracellular polymeric substances (EPS) – including polysaccharides, lipids, proteins, and extracellular DNA – that together constitute a biofilm matrix. As the meshwork of EPS builds up, cells are encased within the matrix and become immobilized. Over time, sessile cells on the biofilm outskirts can occasionally detach, regain motility, and return to a planktonic mode of growth. These freed bacteria can then go on to form new biofilm microcolonies on other sites of the surface.^{45–50}

During arthroplasty, *C. acnes* may be unwittingly transferred from the dermis to the surgical site, where it adheres to the implant surface and begins to form a biofilm once a critical microbial density is achieved. Once the biofilm has matured, it can provide *C. acnes* with a hypoxic environment that is favorable for survival, act as a barrier to antimicrobials and immune cell infiltration, and confer protection from shear stresses caused by joint movement.^{45,51} Furthermore, the metabolic activity of *C. acnes* is greatly reduced in a mature biofilm, which can mask the microorganism from detection.⁵² *C. acnes* biofilm formation has been observed on a wide range of materials of variable shape and hardness. The chemical composition of the *C. acnes* biofilm, the genes encoding it, and the factors that regulate it are not well understood.⁴⁵

C. acnes biofilms are clinically important as they appear to hinder the host wound repair process in a manner that is unrelated to the inherent pathogenicity of planktonic *C. acnes* cells. For example, the mannose content in *C. acnes* biofilms are much higher than the sum total produced by an equivalent cell count of planktonically-grown *C. acnes*.⁴⁵

Mannose is known inhibit the synthesis of hyaluronan – a glycosaminoglycan and major extracellular matrix scaffold component that is involved in the formation of granulation tissue (i.e. new connective tissue and capillaries that form a scaffold for wound healing).⁵³

The ability of *C. acnes* to form biofilms within artificial joints is arguably the main reason PJIs are so difficult to manage. While several widely used antimicrobials are effective against planktonic *C. acnes* at sub-micromolar concentrations (daptomycin, vancomycin, levofloxacin, penicillin, clindamycin, and ceftriaxone), they are clinically ineffective at eradicating *C. acnes* embedded in biofilms.⁵¹ Rifampicin appears to be one of the most effective antibiotics at killing sessile bacteria that live within biofilms, but reports have shown it is unable to consistently eradicate *C. acnes* in its entirety. Moreover, a recent study found several clinical *C. acnes* strains have developed resistance to rifampicin.⁵⁴

C. acnes biofilms can harbor other pathogenic microbes involved in PJI and enhance their virulence. For example, *C. acnes* is commonly co-isolated with *Staphylococcus aureus* in polymicrobial PJIs, and the secretion of a *C. acnes* CAMP factor has been shown to cause a two-fold increase in the hemolytic and cytolytic activity in *S. aureus*.⁵⁵ Furthermore, *C. acnes* appears to facilitate long-term survival of *S. aureus* by expressing a gene that promotes porphyrin metabolism into coproporphyrin III, which contributes to the aggregation *S. aureus* cells and the formation of a polymicrobial biofilm.⁵⁶ Tyner and Patel (2016) showed that *S. aureus* survival rates were indeed higher in polymicrobial biofilms containing *C. acnes* relative to biofilms containing only *S. aureus*.⁵⁷

1.2.4 Diagnostic Challenges

C. acnes PJIs are difficult to diagnose, as symptoms of infection are typically not present until weeks or months after the initial operation.²⁵ It is possible that *C. acnes* infections are initially indolent because microbial expansion requires low oxygen conditions generated by the metabolism of surrounding host tissues.

Common inflammatory biomarkers such as C-reactive protein, erythrocyte sedimentation rate, and white blood cell count cannot reliably detect a *C. acnes* infection.^{58,59}

Consequently, routine detection of *C. acnes* infections involves anaerobic culturing of intraoperative biopsy samples – a process that requires a minimum of 10 days.^{12,60–62} This slow detection approach is not only extremely slow, but it is also subject to the high possibility of contamination during sample collection and culture. Consequently, an estimated 20% of PJI cases involving *C. acnes* are false positive diagnoses.⁶³

Recently, a genetic-based diagnostic assay has been developed for confirming a *C. acnes*-associated infection with greater speed (< 24 hours) and accuracy compared to routine microbial cultures.⁶⁴ This assay involves a two-step approach. First, a region of the *C. acnes* 16S rRNA gene with high species-specificity is amplified by polymerase chain reaction. Next, the presence of a uniquely *C. acnes* nucleotide polymorphism site is confirmed in this amplified region by enzymatic digest with *HindIII*. While this detection assay is highly sensitive and specific for *C. acnes*, it has yet to realize widespread clinical adoption due to prohibitive machinery costs and the technical expertise required to obtain a diagnosis. The ideal detection approach for *C. acnes*-associated PJI would be a point-of-care assay that can provide an accurate diagnosis while the patient is on the operating table, allowing surgeons to employ prophylactic measures during surgery.

1.3 Current models of PJI

1.3.1 Overview

Models are important in that they allow researchers to directly investigate disease characteristics and potential treatments. Models of PJI provide a preclinical landscape for the development of novel anti-infection therapies, screening of potential biomarkers, and validation of current clinical approaches to managing infection. In the 2019 Proceedings of the International Consensus on Orthopedic Infections, the scarcity of joint infection models was identified as an unmet need in orthopedic research.⁶⁰ The development of novel models with high preclinical validity and are easy to adopt is imperative to further our understanding of PJI. Existing models of PJI can be classified as either *in vivo*

(animal models) or *ex vivo* (cell culture-based models), both of which include distinct advantages and limitations.

1.3.2 Animal Models

Large animal species have been previously used to model orthopedic infection in humans. The impact of microbial biofilms on joint infection has been studied in goats and sheep^{65,66}, and the risk factors of infection have been extrapolated retrospectively from horses.⁶⁷ However, the use of large animals is not routinely adopted in the study of orthopedic infection due to prohibitive costs and ethical concerns.⁶⁸

The use of smaller animals as models, such as mice and rabbits, is more routine. While the types of implant mimetics and the method of introducing these implants may differ amongst technicians, several studies have successfully replicated microbial biofilm formation in these animals.^{52,69,70} However, small animal models of PJI generally provide an inaccurate reflection of PJI in human patients due to substantial physiological differences between species.

There are several limitations in using small animals to model a *C. acnes* associated PJI. First, mice and rabbits cannot maintain a *C. acnes* PJI the way it is maintained in humans, as their sebaceous glands contain little to no triglycerides that normally support *C. acnes* metabolism in humans.⁷¹ Second, mice and rabbits have historically co-evolved with a different set of resident microorganisms compared to humans and therefore have different joint microbiotas.⁷² *C. acnes* is known to interact with other microorganisms during infection processes like biofilm formation, so this discrepancy between species may engender misleading results. Third, there is no evidence to suggest that small animal joints have a similar degree of avascularity to larger human joint implants. Fourth, differences in immune responses between humans and small animals can drastically affect how infection progresses. There is evidence to suggest that *C. acnes* interacts with the host immune system, particularly with macrophages, during PJI.^{27,71} However, important human immune regulators may not be present in small animals, particularly in immunocompromised lab animals kept in a sterile environment. For example, memory CD8+ T cells – the first responders to infection – have been measured to be at nearly

undetectable levels in adult lab mice.⁷³ This suggests that essential immune functions such as the foreign body response may be either missing or attenuated in small animals.

In general, preclinical research done using animal models translate poorly in patients. It is predicted that only an estimated one-third of animal studies ever translate into human trials and one-tenth into clinical use in patients.^{74,75}

1.3.3 *Ex vivo* Models

An *ex vivo* model is a system in which cells are isolated from their natural physiology and cultured under external laboratory conditions. Compared to animal models, an *ex vivo* model generally offers superior reproducibility since experiment parameters can be controlled. However, an *ex vivo* model also alters the cells' natural environment, and key cellular responses and molecular interactions may be absent as a result.

To date, several *ex vivo* models have been developed for investigating *C. acnes*-associated PJIs. Most of these models are simple 2D bacterial growth assays designed to study the constituents of the *C. acnes* biofilm and the mechanisms of their formation.^{45,76} *Ex vivo* models involving co-cultures of *C. acnes* and human cells have also been developed. For example, Aubin *et al.* used a simple broth culture assay to study gene expression changes in *C. acnes* following engulfment by osteoblasts and osteoclasts.⁷⁷ Fischer *et al.* used a similar system to assess the viability and proliferation of *C. acnes* following engulfment by THP-1 human monocytes/macrophages.⁷⁸

1.3.4 *In vitro* Models

To our knowledge, there is currently no model of PJI designed to study the interactions between microbial pathogens and human connective tissue in a 3D environment that is representative of human joint physiology. Such a model would necessitate recreation of the joint-implant microenvironment under controlled laboratory settings.

The joint capsule is mainly comprised of connective tissue (i.e. tendon, ligaments, bone, and cartilage). Given that the most abundant protein in connective tissue is collagen, and prosthetic encapsulation is solely a connective tissue process, a collagen-based model of PJI would likely provide a good degree of physiological relevance.⁷⁹ Furthermore, the

polymerization of collagen would encapsulate cells within a 3D scaffold and engender multi-directional cellular interactions similar to those in 3D joint tissues.

This thesis features the development of two novel 3D collagen-based *in vitro* models of *C. acnes*-associated shoulder joint infection, as well as their applications in furthering the understanding of PJI and the therapeutic interventions used to treat PJI.

1.4 Objectives and Rationale

Objective 1

To profile global gene expression changes in human shoulder capsule (SC) fibroblasts and *C. acnes* in response to co-culture in a modified cell-populated collagen lattice system (**figure 1.3**).

Objective 1 Rationale

The cell-populated collagen lattice is a well-established 3D cell culture model routinely used for studying cellular behaviors and gene expression changes in monocultures of connective tissue cells, such as fibroblasts.⁸⁰ We chose to expand the scope of this model to accommodate eukaryotic/prokaryotic cell co-cultures. Capsular fibroblasts from the shoulder joint are hypothesized to interact directly with *C. acnes* during PJI, so there is physiological relevance in mapping the gene expression changes in these cells. We anticipate this experiment will reveal key molecular pathways of the PJI process, as well as novel diagnostic biomarkers of early infection.

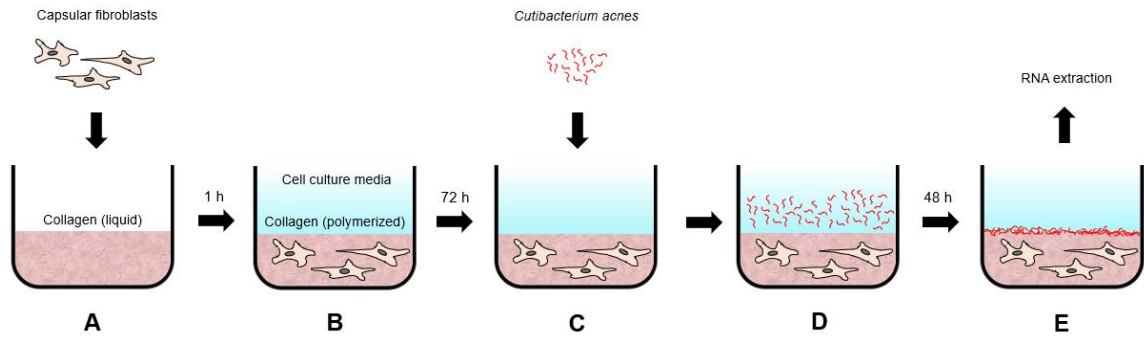


Figure 1.3. Fibroblast-bacteria Co-culture in 3D Collagen (FBCC) model.

(A) Patient-derived shoulder capsule fibroblasts were suspended in a collagen solution that polymerizes into a solid disc-shaped 3D lattice. **(B)** The collagen lattices were incubated in cell culture media under 5% CO₂ and 37°C, allowing fibroblasts to adjust to the 3D lattice environment. **(C)** Following a period of cell culture, the original media was replaced by fresh media containing an inoculum of *Cutibacterium acnes*. **(D)** The fibroblasts in collagen and *C. acnes* in media were incubated under hypoxic conditions (2% O₂). **(E)** *C. acnes* in the media replicate and colonize the collagen surface, where they can interact with the immobilized fibroblasts. Following a period of co-culture, total RNA from both the fibroblasts and *C. acnes* was extracted from the collagen lattice.

Objective 2

To develop and optimize a 3D bioartificial human tissue model that can accurately recapitulate the microenvironment surrounding a surgical implant within an infected shoulder joint (The Shoulder Joint Implant Mimetic, **figure 1.4**).

Objective 2 Rationale

To our knowledge, the S-JIM is the world's first *in vitro* model of PJI. It is a system whereby cells are cultured under artificially created conditions designed to resemble their native joint environment. This model could provide a realistic preclinical landscape for the development of novel anti-PJI therapies, the screening of potential *C. acnes*-associated biomarkers, and the validation of current clinical approaches to managing joint infection. The S-JIM is unique in that it supports a co-culture of anaerobic bacteria and soft bioartificial tissues created using patient-derived capsular fibroblasts. Unlike existing *ex vivo* models of PJI, including the FBCC, cells in the S-JIM are cultured in a 3D extracellular matrix with varying oxygen levels per layer. This is hypothesized to be representative of the environment generated by periprosthetic tissues surrounding an implant. Compared to existing animal models of PJI, we anticipate the S-JIM will provide fewer technical challenges, allow for faster data generation, engender less experimental replication variability and bypass the complicated issue of translating research findings from animal test subjects to human patients.

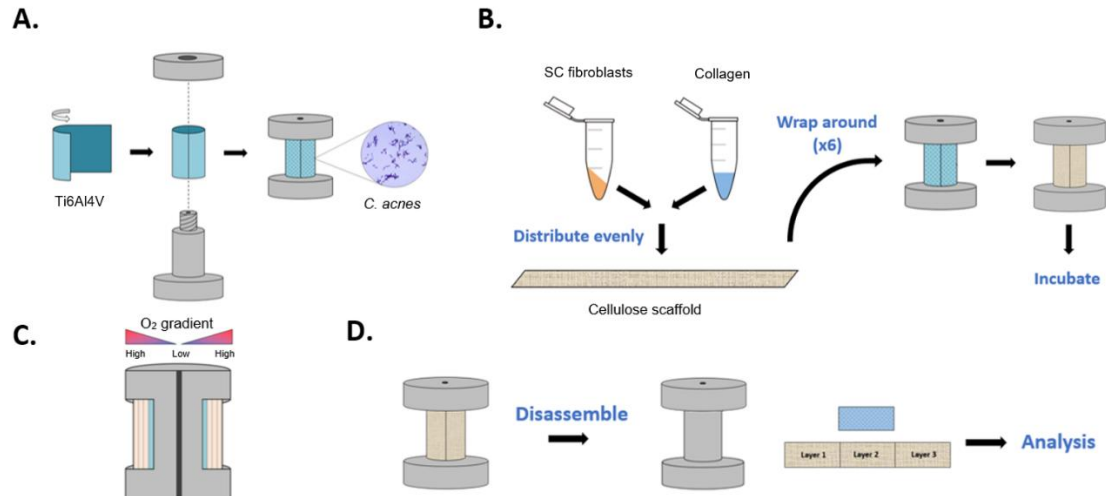


Figure 1.4. Shoulder-Joint Implant Mimetic (S-JIM) model.

The S-JIM is a 3D *in vitro* cell culture system of *C. acnes* and primary SC fibroblasts derived from shoulder arthroplasty patients. **(A)** An implant mimetic was constructed by attaching a sheet of surgical titanium alloy onto a custom-designed mandrel. **(B)** SC fibroblasts were distributed into six collagen-impregnated cellulose scaffold strips and wrapped around the core of this mandrel in several successive layers to generate a cylindrical 3D bioartificial tissue construct. **(C)** This tissue construct was incubated under atmospheric oxygen levels, 5% CO₂, at 37°C. The growth of SC fibroblasts induced a decreasing oxygen accessibility gradient from the external to internal cell layers. **(D)** At various timepoints post-incubation, the strips of bioartificial tissue were unrolled, sectioned by circumferential layer, and subjected to fluorescence confocal microscopy and quantitative PCR analyses of gene expression to assess for cellular responses at different layers.

Objective 3

To assess the effectiveness of vancomycin prophylaxis in *C. acnes*-associated periprosthetic joint infections using the newly developed S-JIM model.

Objective 3 Rationale

At present, clinical evidence for the prophylactic use of vancomycin in shoulder PJIs is weak due to the lack of controlled retrospective studies with complete datasets and adequate patient sample sizes. An *in vitro* system like the S-JIM can directly assess vancomycin's bactericidal effectiveness under controlled parameters. Advantages of this system include the ability to model the delivery of vancomycin both in powder form and as an intravenous injection.

Objective 4

To determine a *C. acnes*-specific molecular target that can be used for microbial detection by desorption electrospray ionization mass spectrometry (DESI-MS) in the S-JIM.

Objective 4 Rationale

Detecting *C. acnes* in a PJI is challenging due to the absence of routine inflammatory serum biomarkers. DESI-MS can potentially provide a rapid diagnosis of *C. acnes* within an infected joint, based on microbe-specific molecular targets. The first step in realizing DESI-MS as a point-of-care detection assay is to provide proof-of-principle for the existence of a *C. acne* specific molecular target that can reliably differentiate the bacteria from neighboring host tissues.

Chapter 2

2 MATERIALS AND METHODS

2.1 Sample Collection

2.1.1 Primary Human Fibroblasts

Human shoulder capsule (SC) tissue offcuts designated “surgical waste” were excised from patients undergoing shoulder arthroplasties, de-identified and used for research purposes in accordance with Human Subject Research Ethics Board (HSREB) approval (#104888) at St. Joseph’s Health Care London, Canada. Tissue samples were dissected into ~1 mm fragments in a 10 mm petri dish using a scalpel and pair of tweezers. To facilitate the outgrowth of primary shoulder capsule (SC) fibroblasts, the tissue fragments were cultured in Dulbecco’s Modified Eagle Medium (DMEM) supplemented with 8% Gibco™ fetal bovine serum and a 1x Antibiotic-Antimycotic cocktail (100 units/mL of penicillin, 100 µg/mL of streptomycin, and 250 ng/mL of Gibco Amphotericin B) under standard conditions (37° C and 5% CO₂). After 10 to 15 days, tissue fragments were removed and SC fibroblasts that adhered to the petri dish were detached using trypsin and transferred into a T75 flask. DMEM was replaced every 2-3 days and the cells were split in a 1:4 ratio at ~90% confluency every 5-10 days. SC fibroblasts that reached passages 3 to 8 were detached using trypsin, centrifuged at 1500g, and resuspended in DMEM-soy media (DMEM supplemented with 8% fetal bovine serum and 0.4% soytone without the addition of antibiotics/antimycotics). These cells were used in downstream 3D co-culture experiments.

2.1.2 *Cutibacterium acnes*

C. acnes strains ATCC® 6919™ and ATCC® 11827™ were purchased from the American Type Culture Collection. *C. acnes* strain CA01 was isolated from the implant surface of a patient undergoing shoulder arthroplasty at St. Joseph’s Health Care London, Canada. All patient information was de-identified in accordance with HSREB restrictions under protocol #104888. All bacterial strains were stored in liquid nitrogen by flash-freezing. Initial subcultures of *C. acnes* strains were grown in brain heart infusion media

under 0% O₂, 5% CO₂, and 37° C for 3 days prior to use in downstream applications. For experiments involving co-culture with SC fibroblasts, *C. acnes* was grown in DMEM-soy.

2.2 Fibroblast-bacteria Co-culture in 3D Collagen Setup

Primary SC fibroblasts were cultured in fibroblast-populated collagen lattices, as described in Grinnell and Lamke (1984), with minor modifications in cell volumes and concentrations. Briefly, cells were grown in T75 culture flasks were detached using trypsin, centrifuged at 1500G, and resuspended in a 1:9 solution of 10x Waymouth media and Type I rat tail collagen (pre-warmed to ~25° C) at a concentration of 1.5×10^5 cells/mL. 500 uL of this collagen-cell suspension was pipetted into each well of a 24-well tray and allowed to solidify for ~30 minutes in a 37° C cell culture incubator. 1 mL of DMEM supplemented with 8% fetal bovine serum was added to each well and the tray was returned to the incubator. After 72 hours, the original media was replaced by fresh media containing an inoculum of *C. acnes* at 5×10^6 bacteria/mL. Cells were cultured for 48 hours in a hypoxic chamber (2% O₂) at 37° C prior to collection.

2.3 Shoulder-Joint Implant Mimetic Model Setup

Primary SC fibroblasts grown in T75 culture flasks were detached using trypsin, centrifuged at 1500G and resuspended in a 1:9 solution of 10x Waymouth media and Type I rat tail collagen (pre-warmed to ~25° C) at a concentration of 2.5×10^6 cells/mL. 200 uL of this collagen-cell suspension was pipetted into each trough of the strip casting tray (**figure 4.1A**) and immediately covered with strips of paper (dimensions 8 x 112 mm) comprised of cellulose fibers (Miniminit, ON). The collagen-cell mixture in each trough was evenly distributed into the cellulose strips by rolling the cell spreader (**figure 4.1B**) along the length of each trough. The strip casting tray containing the cell-infiltrated scaffolds was then transferred to a sealed sterile container and placed in a 37° C cell culture incubator for 30 minutes to allow for collagen polymerization. Polymerized strips were carefully removed from the strip casting tray using a pair of tweezers, transferred to

a six-well cell culture tray containing pre-warmed DMEM-soy media, and returned to incubate at 37° C for an additional 48 hours.

Log-phase *C. acnes* was suspended in a 1:9 solution of 10x Waymouth media and Type I rat tail collagen (pre-warmed to ~25° C) at a concentration of 5.0×10^6 bacteria/mL and evenly distributed into an 8 x 17 mm cellulose scaffold strip using the same approach described above. This strip was wrapped around the titanium surface of the S-JIM mandrel (**figure 4.1C**) using the strip rolling tray (**figure 4.1D**) to generate a single-layered coating of *C. acnes*. Six additional strips containing SC fibroblasts were wrapped in succession around the S-JIM mandrel. The wrapped biocomposite mandrel was placed in the well of a six-well tray containing 10 mL of DMEM-soy media and incubated for 96 hours under 5% CO₂ at 37°C.

In S-JIM experiments involving the direct application of vancomycin, ~50 mg of vancomycin hydrochloride powder (McGuff Medical Products) was directly applied on top of the *C. acnes*-containing scaffold strip prior to wrapping. In S-JIM experiments modelling the intravenous application of vancomycin, wrapped S-JIM mandrels were cultured in media containing vancomycin at concentrations of 5 and 20 µg/mL, representing the clinical consensus for the initial and trough serum concentrations during infection prophylaxis.^{81,82} After 96 hours of incubation, all strips were unwrapped and the *C. acnes*-containing strip was briefly vortexed in 10 mL of DMEM-soy media. An aliquot (100 µL) of this media was spread onto a brain heart infusion agar plate and cultured anaerobically for 7 days, after which the number of colony-forming units were calculated.

2.4 Desorption Electrospray Ionization Mass Spectrometry

DESI-MS imaging was performed on a Quadrupole-Time-of-Flight Mass Spectrometer (Xevo G2-XS, Waters), using a solvent mixture of 95:5 methanol:water, spiked with 150pg/µL of Leucine Enkephalin, at a flow rate of 1µL/min. All data was collected in the negative ion mode over a mass range of m/z 100-1000, with a voltage of 4.2kV applied to

the spray, a nebulizer gas pressure of 72psi and an ion block temperature of 150°C. S-JIM strips, embedded with *C. acnes* and/or SC fibroblasts according to the S-JIM protocol, were taped to glass microscope slides and experimental samples were smeared, using a plastic pipette tip, directly on top of each strip as well as on a blank slide. Strips were left to dry prior to analysis. Slides were then placed on a 2D translational stage in front of MS inlet and rastered underneath the solvent spray at a rate of 100µm/s. Images were generated using High Definition Imaging software (Waters) at a resolution of 100µm×100µm. All DESI-MS handling and analysis were performed by the Zarrine-Afsar lab from the University Health Network, Toronto, Canada.

2.5 Quantification of Gene Expression

2.5.1 RNA Extraction from FPCL Samples

FPCL samples were excised from the culture tray using a scalpel and submerged in a 1:1 volume of TRIzol™ Reagent. Samples were incubated at room temperature for ~2 hours until all visible collagen-cell fragments were dissolved. The resulting suspension was needle aspirated thrice to ensure complete lysis of cell membranes. RNA was isolated using the Direct-zol RNA MiniPrep kit (Zymoresearch) according to the manufacturer's instructions.

2.5.2 RNA Extraction from S-JIM Samples

S-JIM strips were unraveled from the mandrel using a pair of tweezers and sectioned by their circumferential layer during culture. Each strip section was submerged in 500 µL of TRIzol™ Reagent and repeatedly vortexed for ~15 seconds at 30 minute intervals over ~2 hours. S-JIM strips were subsequently removed, and RNA was isolated using the Direct-zol RNA MiniPrep kit (Zymoresearch) according to the manufacturer's instructions.

2.5.3 cDNA Synthesis

Total RNA concentration and quality ($A_{230:260}$ and $A_{260:280}$) were determined using a NanoDrop-1000 spectrophotometer (ThermoFisher Scientific). 200 ng to 1 μ g of total RNA was reverse transcribed into cDNA using the High-Capacity cDNA Reverse Transcription Kit (ThermoFisher Scientific) according to the manufacturer's instructions.

2.5.4 Real Time PCR

cDNA was diluted two-fold in RNase/DNase-free water and 4.5 μ L of this dilution was loaded in triplicate into MicroAmp Optical 384-well reaction plates (Life Technologies). TaqMan gene expression assays (Life Technologies) were used to measure expression of genes of interest in accordance with the manufacturer's instructions. All gene expression levels were assessed relative to expression of the "housekeeping" gene *RPLP0* (encoding Ribosomal Protein Lateral Stalk Subunit P0), as it displayed the least degree of variability across treatment groups. PCR reactions were carried out for 40 cycles of denaturation (95°C for 1 second) and annealing/extension (60°C for 20 second). Relative quantification was calculated using the $\Delta\Delta C_t$ method.

2.5.5 Statistical Analysis

Statistical analysis was conducted using Prism8 (GraphPad) software. Ordinary one-way ANOVA with Tukey's multiple comparisons test was used to identify significant gene expression changes in SC fibroblasts cultured with and without *C. acnes*. Statistical significance between grouped means is indicated as follows: * $p < 0.05$, ** $p < 0.01$, *** $p < 0.001$. All error bars represent a 95% confidence interval in which the true mean of the dataset is represented for each experimental condition.

2.5.6 RNA Sequencing

RNA quality ($A_{260/280}$ and $A_{260/230}$ values between 1.8 and 2.0) and yield (>100 ng/ μ L) were confirmed for all experimental samples using the Agilent 2100 Bioanalyzer. From each sample, ribosomal RNA was isolated from 1.0 μ g of total RNA and RNA libraries were prepared using the Illumina NextSeq Mid Output Kit (Vazyme VAHTS Total RNA-seq (H/M/R) Library Prep Kit for Illumina®). The resulting RNA libraries were

sequenced using the NextSeq 550 System and the RNA library preparation was analyzed using Partek Flow® data analysis software. In brief, raw sequencing reads were aligned to the human reference genome (hg38) using the Spliced Transcripts Alignment to a Reference (STAR) tool. The aligned reads were screened for noise at a minimum threshold of 50 reads/gene and normalized by Counts Per Million (CMM + 1). Differential analysis of gene expression was performed using Gene Specific Analysis (GSA). Inclusion criteria for downstream analysis consisted of $p \leq 0.01$ and fold-change in gene expression of ≥ 2.0 or ≤ -2.0 . All heat-maps, gene set enrichment, and pathway enrichment data were generated using internal Partek Flow® data analysis software.

2.6 S-JIM Cell Imaging

2.6.1 EF5 Hypoxia Labelling

Sixteen hours prior to staining, EF5 – a small molecule with hypoxia-inducible cell binding affinity – was added to the S-JIM cell culture media to a final concentration of 100 μM . S-JIM strips were unraveled from the mandrel using a pair of tweezers, sectioned by their circumferential layer during culture, and immediately fixed in 4% paraformaldehyde for 10 minutes. Following fixation, section samples were permeabilized by 0.2% Triton X for 20 minutes, blocked with 5% bovine serum albumin and stained with 25 $\mu\text{g/ml}$ Cy3-conjugated anti-EF5 antibody (Millipore Sigma) at 4° C overnight. All samples were washed thrice in phosphate-buffered saline (PBS) buffer for 5 minutes after each of the abovementioned steps. Processed samples were imaged using a A1R HD25 confocal microscope (Nikon Imaging).

2.6.2 Live-Dead Mammalian Cell Labeling

S-JIM strips were unraveled from the mandrel using a pair of tweezers, sectioned by their circumferential layer during culture, and washed briefly in PBS. Section samples were then stained with 3 μM calcein-AM (live stain) and ethidium homodimer-1 (dead stain) for 20 minutes, washed briefly in PBS, and imaged using a A1R HD25 confocal microscope (Nikon Imaging).

2.6.3 Scanning Electron Microscopy

Titanium foil samples were carefully removed from the S-JIM mandrel following cell culture and immersed in 2.5% glutaraldehyde constituted in Sorensen's buffer (16 mM KH_2PO_4 + 117 mM Na_2HPO_4 , pH = 6.0). Samples were fixed for 2 hours at room temperature and washed 3 times with Sorensen's buffer (5 minutes per wash). Following fixation, samples were initially dehydrated in progressively higher concentrations of ethanol (25% → 50% → 70% → 90% → 100%) and further dehydrated in hexamethyldisilazane before being processed in a critical point dryer. Once completely desiccated, samples were mounted on carbon-taped aluminum stubs and gold/palladium-sputtered at 15 mA for 4 minutes. All imaging and image analysis were performed using a Hitachi S-3400N with the assistance of Karen Nygard and Reza Khazaei from the Integrated Microscopy Facility, Biotron, Western University.

Chapter 3

3 FIBROBLAST-BACTERIA CO-CULTURE IN 3D COLLAGEN (FBCC)

3.1 Validation of Model and Suitable Housekeeping Gene in SC Fibroblasts Following Co-culture with *C. acnes*

The impact of *C. acnes* on the gene expression of human shoulder fibroblasts has not been previously studied, despite the proximity of these cells in an infected joint capsule. The FBCC model was developed for real time PCR (**methods 2.5.4**) and RNA sequencing analyses (**methods 2.5.6**) of gene expression changes in SC fibroblasts following co-culture with *C. acnes* in a 3D collagen lattice (**methods 2.2**).

All experiments involving the FBCC model were conducted under 2% O₂ as the hypoxic environment is representative of the post-operative shoulder joint and enables the proliferation of *C. acnes* and SC fibroblasts. We selected 24 and 48 hours as the co-culture durations as the *C. acnes* strains achieved *in vitro* log-phase growth during this timeframe (**figure 3.1**). Three *C. acnes* strains – ATCC 6919, ATCC 11827 (dermally-derived isolates), and CA01 (patient-derived biopsy from the site of shoulder PJI) – were used in the co-culture experiments.

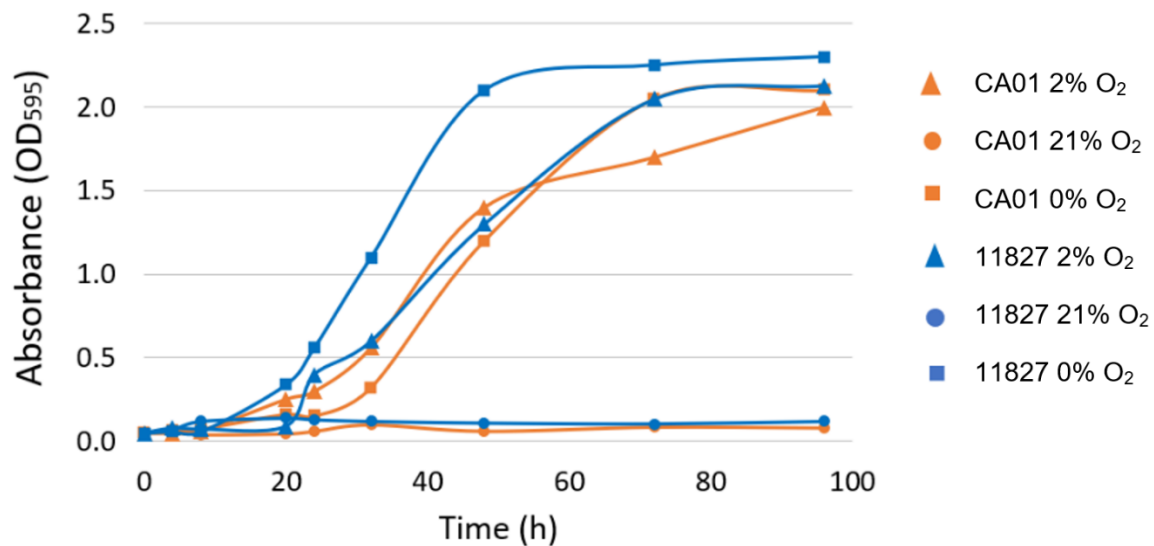


Figure 3.1. *In vitro* Growth Curve of *C. acnes*.

The growth of *C. acnes* strains CA01 and ATCC 11827 was monitored under 0%, 2%, and 21% oxygen cell culture conditions over 96 hours. Each datapoint represents an average absorbance reading of three replicates ($n = 3$).

Given that this is the first reported co-culture experiment involving *C. acnes* and SC fibroblasts, reference gene(s) that were previously determined to exhibit stable expression in human cells had to be revalidated to rule out the possibility of interference with *C. acnes* transcripts. The expression of three housekeeping genes were evaluated – *RPLP0* (*Ribosomal Protein Lateral Stalk Subunit P0*), *GAPDH* (*Glyceraldehyde 3-phosphate dehydrogenase*), and *ACTB* (*Beta-actin*) – for their suitability to serve as reference genes in our real-time PCR experiments. In theory, the expression of a housekeeping gene should remain constant across all treatment and control conditions. However, the expression of *GAPDH*, *ACTB*, and *RPLP0* varied significantly relative to one another in SC fibroblasts cultured with and without *C. acnes* (**figure 3.2A**).

To determine the gene with the smallest change in expression between experimental and control conditions, the consistency in cycle threshold values was assessed for the three genes (**figure 3.2B**). *RPLP0* showed the smallest range and variation of cycle thresholds, indicating it was expressed at more consistent levels across control and treatment groups. This result was later confirmed by RNA sequencing, which revealed *RPLP0* gene expression did not change significantly in SC fibroblasts cultured with and without *C. acnes*. Conversely, *GAPDH* and *ACTB* gene expression were upregulated by 2.59-fold and downregulated by 6.26-fold respectively by the presence of *C. acnes*. The real time PCR and RNA sequencing results were consistent with these data. Thus, the expression of all target genes was normalized to *RPLP0* for evaluating differential expression changes in SC fibroblasts.

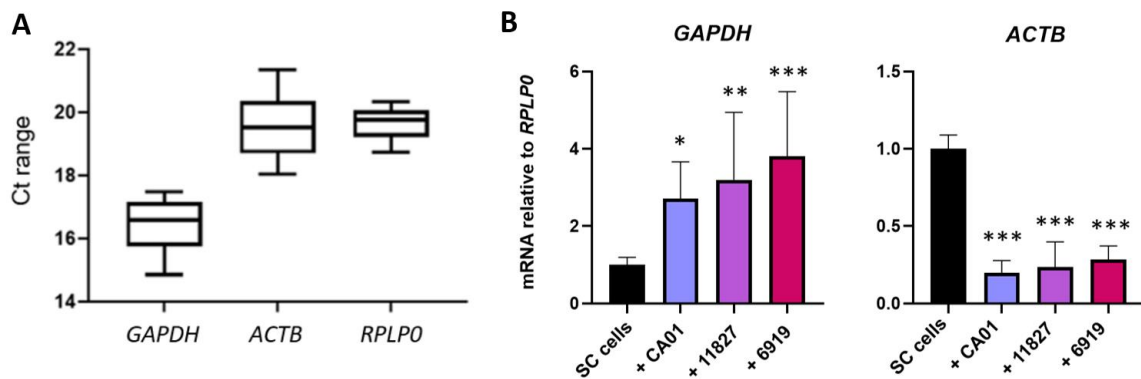


Figure 3.2. Evaluating suitable SC fibroblast housekeeping genes.

(A) The range of cycle thresholds (Ct) from all treatment and control groups were plotted for three putative housekeeping genes *RPLP0*; *GAPDH*, *Glyceraldehyde 3-phosphate dehydrogenase*; *ACTB*, *Beta-actin*. Boxes indicate the interquartile range and capped lines indicate the full range of Ct values. (B) Gene expression of SC fibroblasts co-cultured with *C. acnes* strains CA01, ATCC 11827, and ATCC 6919 in the FBCC system was normalized to the expression of *RPLP0*, *Ribosomal Protein Lateral Stalk Subunit P0*. Significant differences between groups are denoted as * $p < 0.05$, ** $p < 0.01$, and *** $p < 0.001$. All experiments were performed in triplicate ($n = 3$). Error bars indicate 95% confidence intervals.

3.2 Impact of *C. acnes* on SC Fibroblasts Gene Expression

Having established *RPLP0* as a suitable reference gene, it was possible to assess the impacts of *C. acnes* co-culture on SC fibroblast gene expression and determine if these connective tissue cells could detect the presence of *C. acnes* under *in vitro* conditions.

The first step was to assess the expression of genes involved in regulating inflammation, as common inflammatory biomarkers are oftentimes not detected in a *C. acnes* PJI^{58,59} despite inflammation being a general characteristic of microbial infection. The gene expression of the pro-inflammatory cytokines *PTGS2* (*Prostaglandin-Endoperoxide Synthase 2*), *TNF* (*Tumor Necrosis Factor*), *IL6* (*Interleukin 6*), and *CCL2* (*C-C Motif Chemokine Ligand 2*) were reportedly upregulated in prostate epithelial cells in *in vitro* co-culture with *C. acnes*.^{83,84} Conversely, the gene expression of *IL10* (*Interleukin 10*), an anti-inflammatory cytokine, was reportedly downregulated in this simple co-culture model. We chose to investigate the gene expression changes in these cytokines given that they were previously reported to respond to *C. acnes*, and are key regulators of the inflammation response pathway.⁸⁵⁻⁸⁸

The real time PCR data (**methods 2.5.4**) indicated a significant increase in *PTGS2* expression and decrease in *IL10* expression in SC fibroblasts after 24 and 48 hours of co-culture with *C. acnes*. *TNF* expression only increased after 48 hours. For these three genes, changes in expression were more robust at 48 hours compared to 24 hours, indicating the increased sensitivity of SC fibroblasts to *C. acnes* at the longer timepoint. Conversely, *IL6* expression increased after 24 hours but returned to baseline after 48 hours, and *CCL2* expression was unchanged after 24 hours but downregulated after 48 hours. The inconsistency of *IL6* and *CCL2* transcript levels at 24 and 48 hours may be due to temporal regulation of gene expression. Overall, the data were interpreted as indicating a pro-inflammatory response in SC fibroblasts to *C. acnes* infection.

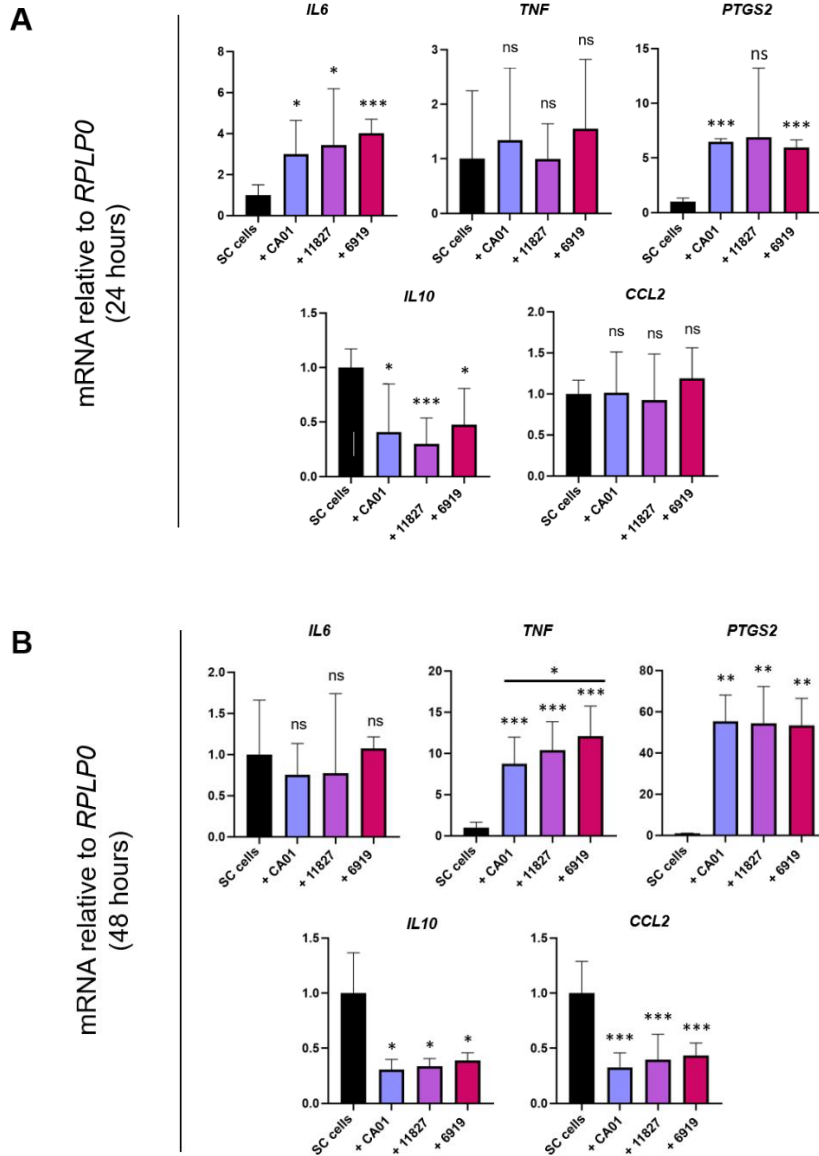


Figure 3.3. *C. acnes* elicits an *in vitro* inflammatory response in SC fibroblasts.

Gene expression of SC fibroblasts co-cultured with *C. acnes* strains CA01, ATCC 11827, and ATCC 6919 in the FBCC system after (A) 24 hours and (B) 48 hours was normalized to the expression of *RPLP0*. Significant differences between treatment groups are denoted as * $p < 0.05$, ** $p < 0.01$, and *** $p < 0.001$. All experiments were performed in triplicate ($n = 3$). Error bars indicate 95% confidence intervals. *PTGS2*, Prostaglandin-Endoperoxide Synthase 2; *TNF*, Tumor Necrosis Factor; *IL6*, Interleukin 6; *CCL2*, C-C Motif Chemokine Ligand 2; *IL10*, Interleukin 10.

Next, the gene expressions of *TLR2* (*Toll-like Receptor 2*), *TLR3* (*Toll-like Receptor 3*), and *TLR4* (*Toll-like Receptor 4*) were assessed to determine whether SC fibroblasts can detect the presence of *C. acnes* on a molecular level (**figure 3.4**). The gene expression of receptor(s) that can specifically detect *C. acnes* was expected to increase given that cellular responses to infection generally involves an amplification in the infection signaling cascade. TLR2 recognizes a broad range of substrates from bacterial cell walls, TLR3 recognizes dsRNA viruses and TLR4 recognizes lipopolysaccharides found on gram-negative bacteria (*C. acnes* is gram-positive).⁸⁹ A ~5 fold increase was observed for *TLR2* expression, whereas a ~5 to 10 fold decrease was observed for *TLR3* and *TLR4* expression after 48 hours of culture.

C. acnes infection has been shown to inhibit wound repair processes like ECM formation, so the expression of genes involved in extra-cellular matrix (ECM) formation – *HAS3* (*Hyaluronan Synthase*), *COL1A1* (*Collagen Type I Alpha 1 Chain*), *COL3A1* (*Collagen Type III Alpha 1 Chain*) – were assessed. All three genes were significantly downregulated in SC fibroblasts after 48 hours of co-culture with *C. acnes* (**figure 3.5**).

The real-time PCR analyses of gene expression demonstrated that multiple cellular processes in SC fibroblasts react to the presence of *C. acnes*. However, the analyses only observed a small subset of genes involved in these cellular processes and may not be representative of the overall response. It was also unclear whether downregulation of extracellular matrix genes (*COL1A1*, *COL3A1*, and *HAS3*) and toll-like receptor genes (*TLR2* and *TLR4*) were the result of specific signaling pathways induced by *C. acnes* or a general repression of non-essential genes due to infection.

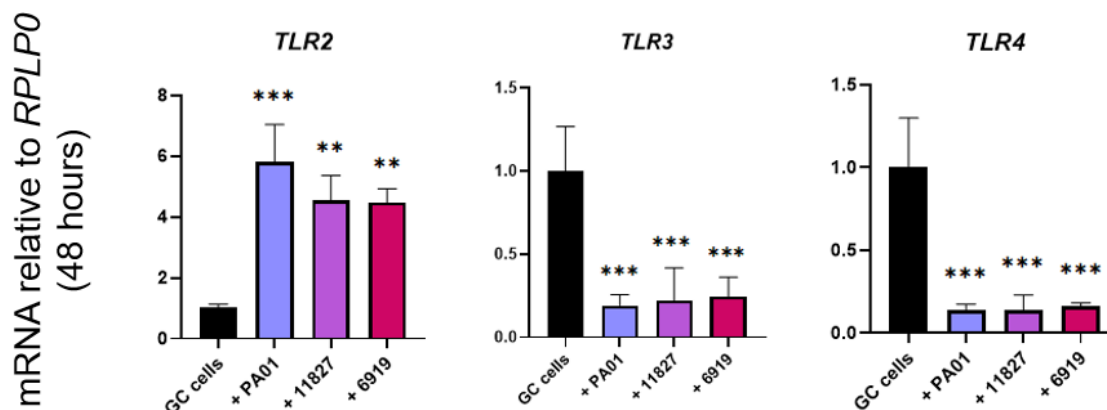


Figure 3.4. Expression of toll-like receptor genes are suppressed in SC fibroblasts following co-culture with *C. acnes*.

Gene expression of SC fibroblasts co-cultured with *C. acnes* strains CA01, ATCC 11827, and ATCC 6919 in the FBCC system after 48 hours was normalized to the expression of *RPLP0*. Significant differences between treatment groups are denoted as * $p < 0.05$, ** $p < 0.01$, and *** $p < 0.001$. All experiments were performed in triplicate ($n = 3$). Error bars indicate 95% confidence intervals. *TLR2*, *Toll-like Receptor 2*; *TLR3*, *Toll-like Receptor 3*; *TLR4*, *Toll-like Receptor 4*.

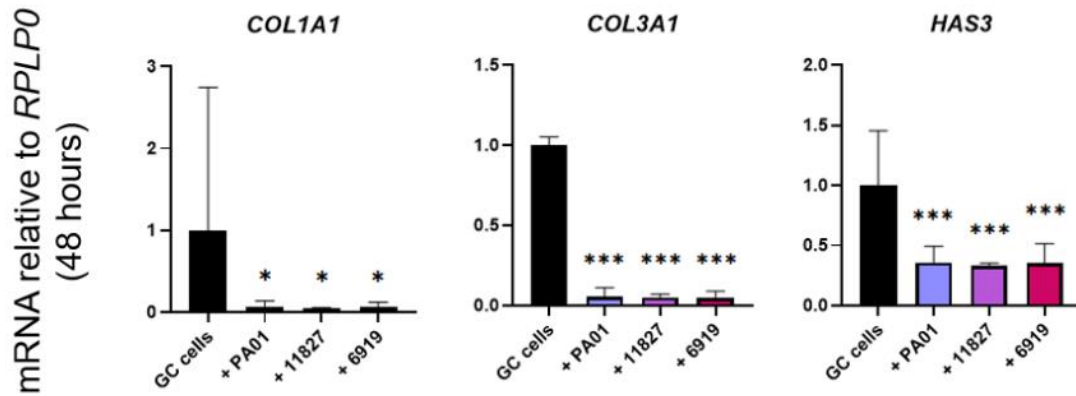


Figure 3.5. Expression of extracellular matrix genes are suppressed in SC fibroblasts following co-culture with *C. acnes*.

Gene expression of SC fibroblasts co-cultured with *C. acnes* strains CA01, ATCC 11827, and ATCC 6919 in the FBCC system after 48 hours was normalized to the expression of *RPLP0*. Significant differences between treatment groups are denoted as *p < 0.05, **p < 0.01, and ***p < 0.001. All experiments were performed in triplicate (n = 3). Error bars indicate 95% confidence intervals. *COL1A1*, Collagen Type I Alpha 1 Chain; *COL3A1*, Collagen Type III Alpha 1 Chain; *HAS3*, Hyaluronan Synthase 3.

3.3 Net Changes in SC Fibroblast Gene Expression in Response to a *C. acnes* Infection

To gain a genome-wide perspective of gene expression changes induced by *C. acnes*, a transcriptomic profile was generated for SC fibroblasts, using the RNA sequencing approach described in **methods 2.5.6**. SC fibroblast cultures from three different arthroplasty patients (N = 3), and two *C. acnes* strains – ATCC 11827 and CA01 – were included in this experiment.

Total extracted RNA was processed by the London Regional Genomics Centre. In brief, eukaryotic rRNA was depleted, the remaining mRNA and other transcripts were reverse transcribed, sequenced, and aligned to a human reference genome (hg38 - Ensembl Transcripts release 99). Raw transcript reads collectively aligned to 15,860 genes from the human genome, with the expression of 4889 genes being significantly altered ($p < 0.01$) by at least a factor of 2 between SC fibroblasts cultured with *C. acnes* and SC fibroblasts cultured without *C. acnes*. The media pH and oxygen concentration were kept constant at pH = 7 and 2% O₂ in the FBCC system during co-culture.

A heatmap of significant gene expression changes ($p < 0.01$) was generated to visualize differential expression profiles across the experimental samples (**figure 3.6**). The nine experimental samples were sorted into two main groups – SC fibroblasts cultured with *C. acnes* and SC fibroblasts cultured without *C. acnes* – thereby confirming the most significant cause of differential gene expression to be the presence of *C. acnes*.

Most of the differentially expressed genes in SC fibroblasts (77%) were downregulated following co-culture with *C. acnes* (**figure 3.6**). To confirm this, a list of 22 significantly altered cellular pathways ($p < 0.01$) was generated by clustering differentially expressed genes by function (**Table S1**). Twenty of these pathways convincingly showed a net decrease in gene expression activity, thereby supporting our previous observation of gene expression repression mechanism(s). The two pathways that appeared to reflect a net increase in activity were the pro-inflammatory TNF and IL-17 signaling pathways (**figure S1**). In both pathways, genes encoding membrane receptors and intermediate

signaling molecules were downregulated whereas the downstream transcriptional target genes were upregulated.

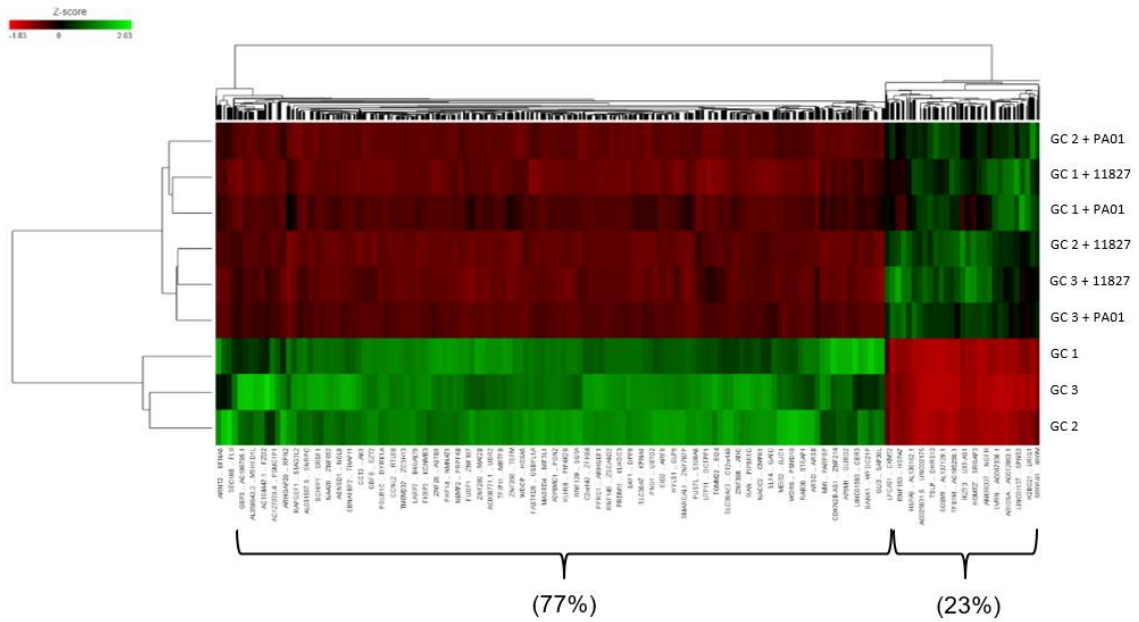


Figure 3.6. Heatmap of differentially expressed mRNA in SC fibroblasts cultured in the FBCC model with or without *C. acnes*.

The mean signal intensities for mRNAs exhibiting $p < 0.01$ are shown following normalization and Z-transformation. Green and red bars represent upregulation and downregulation in gene expression relative to Z-score of 0. Samples used in this analysis include three primary SC fibroblast cell cultures derived from different arthroplasty patients (SC1, SC2, SC3) and two *C. acnes* strain (11827 and CA01). The percentage of genes that were upregulated (23%) and downregulated (77%) with the addition of *C. acnes* are labelled.

Chapter 4

4 Shoulder-Joint Implant Mimetic (S-JIM)

4.1 Model Development and Optimization

The FBCC model is a simple and efficient co-culture system for studying gene expression changes in human fibroblasts during a *C. acnes* PJI. However, the FBCC model does not reflect the oxygen gradient that would be present across connective tissues in a real PJI, given the entire system is kept in a consistent 2% O₂ environment. Furthermore, the FBCC model does not include the presence of an implant mimetic, which is required to initiate a *C. acnes* PJI in mice models. These two limitations of the FBCC model may result in unrepresentative cellular responses to a *C. acnes* PJI.

The S-JIM model was developed to provide a 3D cell culture environment that is more physiologically-representative for the study of PJI. The S-JIM design was adapted from the TRACER cell culture system (Tissue Roll for Analysis of Cellular Environment and Response).⁹⁰ TRACER was originally developed to model tumor behavior under hypoxic conditions. In brief, tumor cells are seeded onto a scaffold strip and rolled around a mandrel core, forming multiple layers of an artificial “3D tumor”. As this “tumor” is cultured, oxygen diffuses through the strips and are progressively metabolized by cells from each successive layer. This generates a gradient of oxygen levels across the outer and inner strip layers, from normoxic to hypoxic cellular environments.^{90,91}

The aim of this project was to cross-purpose the TRACER system into a model of infection by modifying several steps from the original protocol (**Table 4.1**). The process of S-JIM optimization involved several iterations of trial and error. In brief, there were four key considerations in making alterations to the original TRACER protocol:

1. Enabling efficient model setup to increase reproducibility between replicates.
2. Generating an oxygen accessibility gradient across S-JIM layers, with a near-anaerobic inner core to support *C. acnes* proliferation.

3. Creating a microenvironment for adjacent *C. acnes* and SC fibroblasts to interact.
4. Inducing *C. acnes* biofilm formation on the metallic surface of the S-JIM core to mimic infection of a prosthetic implant.

4.2 Custom S-JIM Assembly Tools

A set of 3D-printed cell culture tools was developed to enable efficient and consistent S-JIM setup (**figure 4.1**). The strip casting tray provided a platform for the distribution of cells and collagen into the S-JIM strips. Rapid and even cell seeding distribution was achieved by rolling a cell spreader along the strip length. S-JIM mandrels were designed with a threaded lid and a mandrel base that allowed them to be screwed together into a single unit. This design allowed for easy assembly and removal of coiled metallic foils from the mandrel surface. Scaffold strips were cut to a width of 8 mm to match the mandrel core length and to prevent oxygen leakage from the sides of the mandrel. A video demonstrating S-JIM setup can be found in **Video S1**.

Table 4.1. Modifications to Cell Culture Parameters and Model Setup from the TRACER to S-JIM System.

Parameter	TRACER	S-JIM
Human cell seeding density	1.0 x 10 ⁷⁻⁸ /mL collagen	2.5 x 10 ⁶ /mL collagen
<i>C. acnes</i> seeding density	NA	5.0 x 10 ⁶ /mL collagen
Number of strips per mandrel	1	6
Number of cell-strip layers	6	~25
Strip size	5 x 120 mm	8 x 112 mm
Volume of collagen-cell mix	~90 μ L	~150 μ L

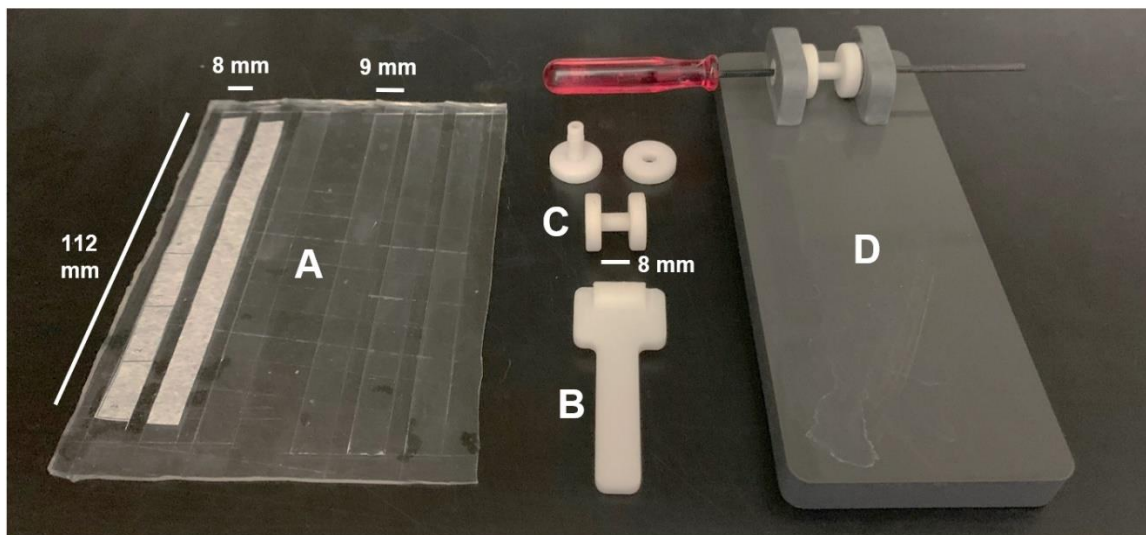


Figure 4.1 Custom-designed cell culture tools for S-JIM setup.

The **strip casting tray (A)** was molded from polydimethylsiloxane (PDMS) – a soft but durable silicon-based polymer with hydrophobic properties. It contains several surface troughs (100 μm deep) that allow collagen-cell suspensions to be evenly distributed onto cellulose scaffold strips using a **cell spreader (B)**. The **S-JIM mandrel (C)** is comprised of a base and an attachable lid, both of which have a hexagonally hollow core parallel to the axis. A single-layer coil of titanium alloy is first secured onto the thinner section of the mandrel base before the lid is re-attached to keep the metal in place. The mandrel is then skewered between the bases of the **strip rolling tray (D)** using a hexagonal screwdriver, whereby rotation of the handle facilitates rapid wrapping of cell-embedded scaffold strips around the mandrel core. All custom-designed tools withstand repeated sterilization by 70% ethanol. All tools aside from the strip casting tray were 3D printed by Lynn Keenlside (Lawson Imaging, St. Joseph's Health Care, London, Canada).

4.3 Generating an Oxygen Accessibility Gradient Across S-JIM Strip Layers

The human connective tissue surrounding a joint capsule is comprised of several layers, and the difference in vascularity between these layers generates a gradient of oxygen accessibility. Given that anaerobes like *C. acnes* preferentially proliferate in hypoxic conditions (**figure 3.1**), the differences in oxygen availability across these tissue layers may contribute to the progression of PJI.

To incorporate this consideration in the S-JIM model, an oxygen availability gradient between ~0% to 21% was generated across the cell-strip layers (**figure 4.2A**). In brief, SC fibroblasts were mixed with collagen and even distributed into the S-JIM strip at different seeding densities, in the absence of *C. acnes*. Oxygen levels at individual layers were assessed by gene expression analyses of *HIF1A* and its downstream transcriptional target, *DDIT3* (**methods 2.5.2**). However, significant differences in oxygen levels were not observed in experiments with initial cell seeding densities between 1.5×10^5 to 2.5×10^6 cells/mL collagen. Increasing the cell density beyond 2.5×10^6 cells/mL collagen was not feasible due to the time and material costs associated with culturing a large quantity of slow-growing primary fibroblasts. Furthermore, SC fibroblasts were larger than tumor cells in the TRACER model (~50 μm in diameter compared to ~10 to 20 μm) and therefore occupied more space in the S-JIM strips.

To increase the contrast in oxygen availability between the inner and outer “tissue” layers in the S-JIM, five additional strips were wrapped around the S-JIM to increase the thickness of the biocomposite mandrel and lower the rate of oxygen diffusion. The additional strips engendered ~25 layers in the S-JIM, in contrast to the 6 layers in the TRACER model. Under these conditions, gene expression analyses of SC fibroblasts in the S-JIM indicated significantly elevated levels of *HIF1A* and *DDIT3* in the inner strip layers relative to outer layers (**figure 4.2B**). This data is consistent with a decreasing oxygen accessibility gradient from the exterior to interior layers. Oxygen levels in SC fibroblasts were further assessed by staining with EF5 – a synthetic compound that preferentially binds to cells in hypoxic conditions. Following incubation with an anti-EF5 cyanine 5 conjugate, the fluorescence intensity in these cells was assessed by confocal

microscopy (**methods 2.6.1**). SC fibroblasts from the inner S-JIM layers exhibited higher fluorescence readings compared to the outer layers (**figure 4.2C**). This data is consistent with a decreasing oxygen availability gradient from the outer to inner “tissue” layers in the S-JIM.

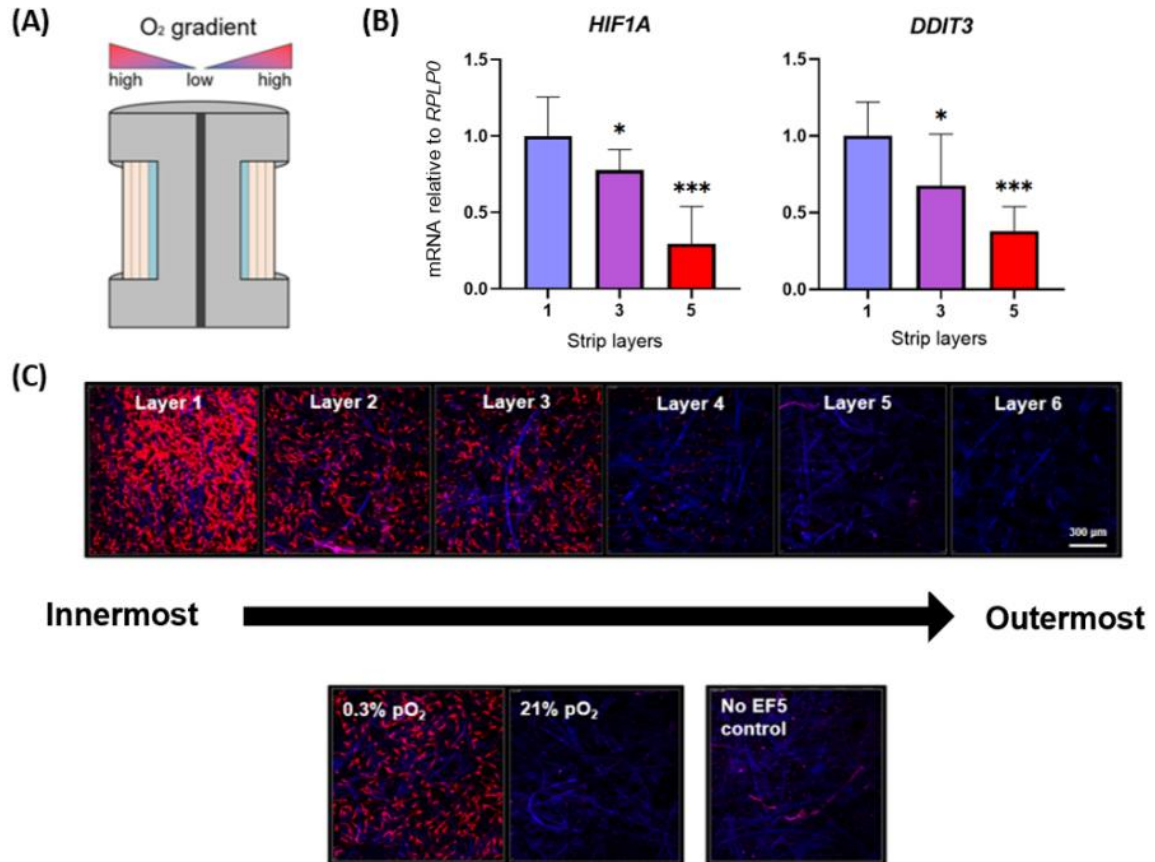


Figure 4.2. Gradient of oxygen levels in the S-JIM.

(A) Theoretical depiction of an oxygen gradient generated by the S-JIM. (B) Gene expression analyses of *HIF1A*, *Hypoxia Inducible Factor 1 Alpha* and its downstream transcriptional target *DDIT3*, *DNA Damage Inducible Transcript 3* in SC fibroblasts were analyzed in the absence of *C. acnes* (n = 3). Error bars indicate 95% confidence interval range. * p < 0.05, *** p < 0.001 (C) SC fibroblasts in the six S-JIM strips were stained with EF5 – a hypoxia probe (red) – and DAPI (blue). Intensity of EF5 signal correlates qualitatively with the relative hypoxia in the cellular environments. Cell-strip controls were cultured under constant 0.3% and 21% O₂ for relative comparison (n = 3).

4.4 *C. acnes* Induces SC Fibroblast Cell Death

Connective tissue necrosis is one of the hallmarks of PJI. To assess the impact of *C. acnes* on the viability of the S-JIM “tissue” layers, SC fibroblasts were labelled with calcein and ethidium homodimer-1. Calcein is a membrane-permeable fluorescein that is activated by intracellular esterase activity and ethidium homodimer-1 is a membrane-impermeable DNA intercalator agent. Only live cells that possess functionally active esterases and intact cellular and nuclear membranes would be labelled with calcein. Conversely, dead or dying cells with no esterase activity and partially lysed cellular and nuclear membranes would be labelled with ethidium homodimer-1.

Calcein and ethidium homodimer-1 labelled SC fibroblasts were imaged by confocal microscopy (**methods 2.6.2**). After 96 hours of co-culture with *C. acnes*, SC fibroblasts from the core S-JIM layers (1 and 2) were predominantly labelled with ethidium homodimer-1, and SC fibroblasts from the outer S-JIM layers (7 and beyond) were predominantly labelled with calcein (**figure 4.3A**). SC fibroblasts in the no bacteria control were predominantly labelled with calcein across all S-JIM layers, thereby confirming that cell viability was not influenced by differences in media and oxygen accessibility between the S-JIM layers (**figure 4.3B**). These results demonstrated that *C. acnes* induces SC fibroblasts cell death, and thereby the necrosis of connective tissue layers that are adjacent to the infection.

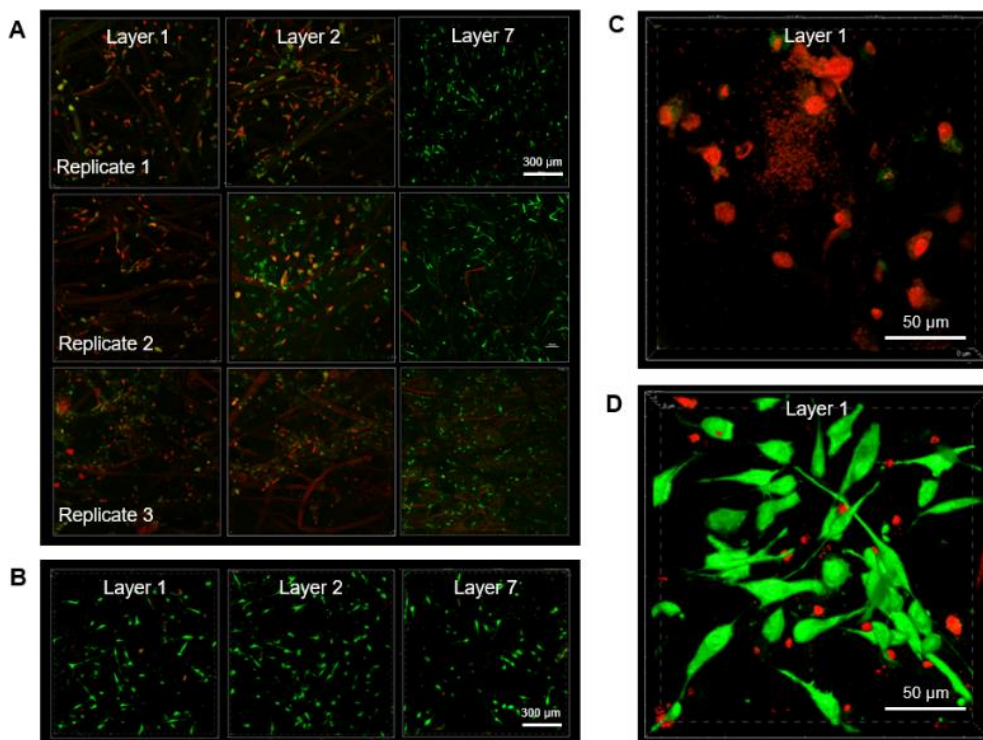


Figure 4.3. *C. acnes* Induces SC Fibroblast Cell Death

Six biocomposite strips embedded with SC fibroblasts were subjected to live-dead staining analyses after 96 hours of incubation in a S-JIM in the presence (**A, C**) or absence (**B, D**) of *C. acnes*. Live SC fibroblasts are labelled with calcein (green) – a cell-permeable dye that is converted to a fluorescent form via intracellular esterase activity. *C. acnes* and dead SC fibroblasts are labelled with the DNA intercalator ethidium homodimer-1 (red). Strip sections are labelled by their respective layer around the S-JIM mandrel, with layer 1 being the innermost layer. All experiments were performed in triplicate (n = 3).

4.5 *C. acnes* Grows on Titanium Alloy Surfaces in an S-JIM but Does Not Form a Biofilm

To determine how *C. acnes* interacts with an implant during PJI, *C. acnes* was co-cultured with SC fibroblasts in the S-JIM, and the Ti6Al4V titanium-alloy surface of the mandrel core was imaged by scanning electron microscopy (**methods 2.6.3**). Individual *C. acnes* cells appeared to form aggregates on the foil surface after 96 hours, but these cells were not encapsulated in an EPS matrix (**figure 4.4**).

Given that *C. acnes* biofilm formation is routinely observed in mouse models⁵², and that these biofilms consist of an extracellular polymeric matrix, several attempts were undertaken to promote *C. acnes* biofilm formation in the S-JIM. The first step involved assessing *C. acnes* biofilm formation on a flat Ti6Al4V surface in the absence of SC fibroblasts. When *C. acnes* was cultured anaerobically in DMEM-soy (the same media used in the S-JIM), cell aggregates were once again observed on the Ti6Al4V surface in the absence of a biofilm matrix. However, when DMEM-soy was replaced with BHI (a routine microbial growth media), *C. acnes* cells appeared to be encapsulated in a gel-like EPS matrix. This matrix was also observed when *C. acnes* was cultured in a 1:1 media combination of DMEM-soy and BHI (**figure 4.5A**). These results indicate that BHI is at least in part necessary for *C. acnes* biofilm formation. However, when BHI or the 1:1 media combination of DMEM-soy and BHI was used to co-culture *C. acnes* with SC fibroblasts in the S-JIM, the EPS matrix was no longer observed.

Additional attempts to generate a *C. acnes* biofilm matrix included diluting the media concentration to promote a “starved” microbial state (**figure 4.5B**), supplementing the culture media with human serum to increase the concentration of coagulant factors in the media (**figure 4.5C**), and increasing the surface roughness of the Ti6Al4V foils to promote bacterial adherence (**figure 4.5D**). However, no convincing evidence of EPS formation was observed after all these attempts.

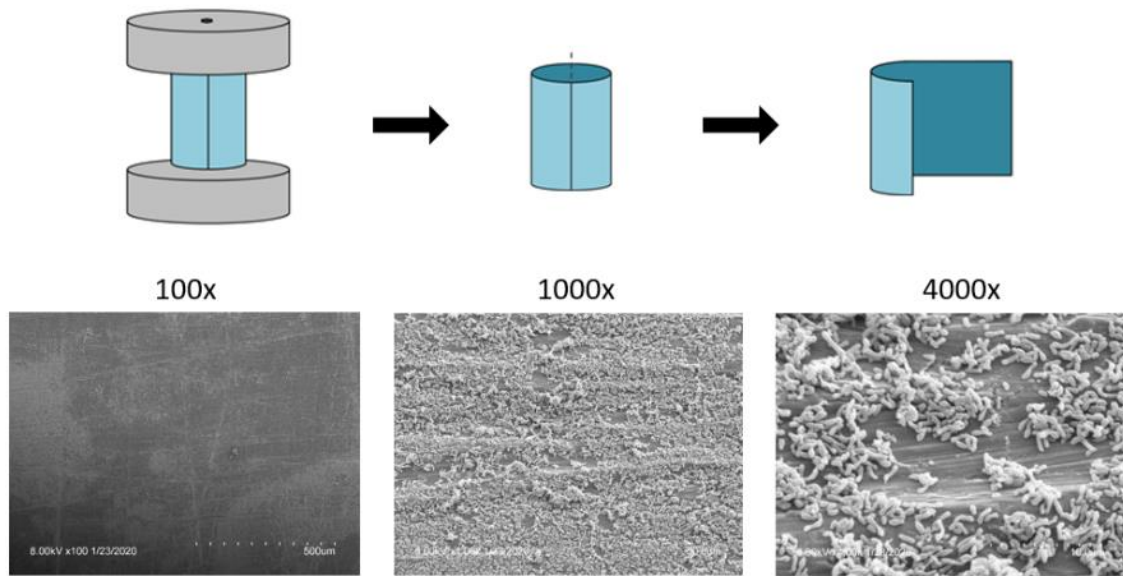


Figure 4.4. *C. acnes* Growth on Ti6Al4V Titanium Alloy Foils in the S-JIM.

Scanning electron microscopy images of *C. acnes* growth on Ti6Al4V foils after 96 hours of co-culture with SC fibroblasts in the S-JIM. Imaging was performed with assistance from the Integrated Microscopy Facility, Biotron, Western University.

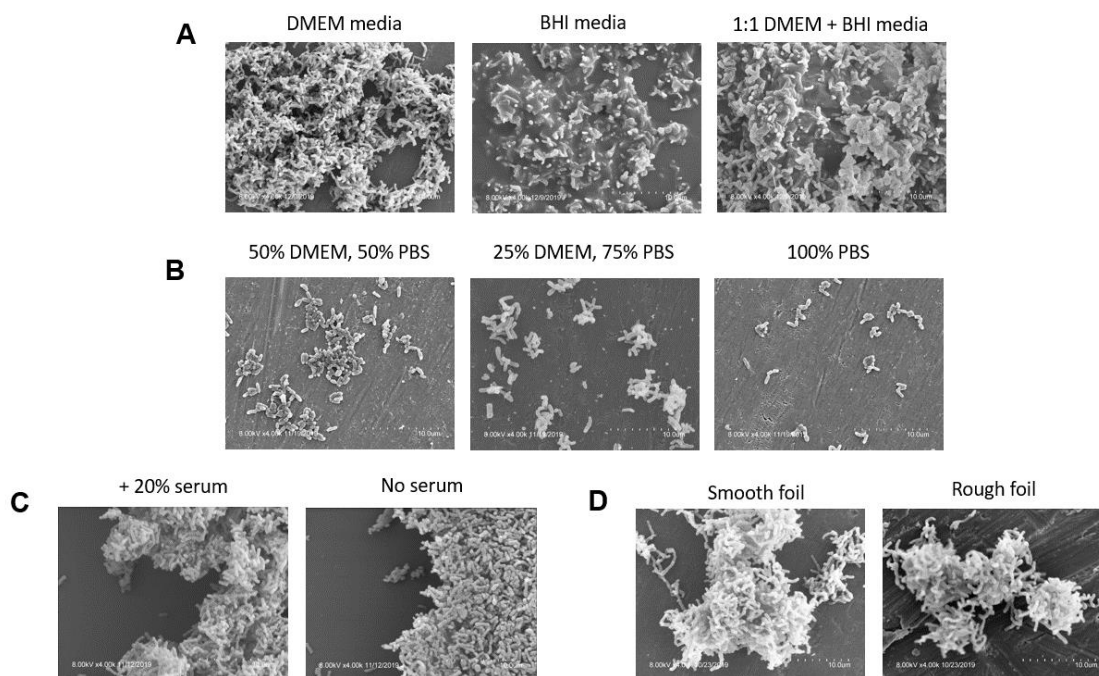


Figure 4.5. *C. acnes* aggregates on the surface of Ti6Al4V titanium-alloy foils.

(A) Scanning electron images of *C. acnes* CA01 on Ti6Al4V titanium-alloy foils cultured in DMEM-soy media, BHI media, and an even mixture of the two for 96 hours. (B) *C. acnes* was cultured for 48 hours with DMEM-soy media, and then for an additional 48 hours in DMEM diluted with an appropriate volume of phosphate-buffered saline. (C) *C. acnes* was cultured in DMEM-soy media supplemented with 20% human serum. (D) *C. acnes* was cultured in DMEM-soy media on a Ti6Al4V foil with an unaltered surface (smooth) and one that has been treated with sandpaper (rough). Imaging was performed with the assistance from the Integrated Microscopy Facility staff, Biotron, Western University.

4.6 Identifying Putative Biomarkers of *C. acnes* PJI

Detecting *C. acnes* in PJIs remains a clinical challenge due to the slow progression of infection and the lack of reliable serum biomarkers. We previously identified a list of SC fibroblast genes that were significantly upregulated in the presence of *C. acnes* using the FBCC system. Several of these genes were hypothesized to be potentially novel biomarkers of *C. acnes* PJI, as they encode secreted proteins that may potentially be detectable in periprosthetic tissues or blood serum. Four of these genes – *Stanniocalcin-1 (STC1)*, *Angiopoietin-like 4 (ANGPTL4)*, *Carboxypeptidase A4 (CPA4)*, and *Neuron derived neurotrophic factor (NDNF)* – were selected for further investigation using the S-JIM model, as their roles in microbial infection is currently unknown.

The changes in gene expression were confirmed by real time PCR (**methods 2.5.2**). In general, the expression of all four genes appeared to be higher in the innermost layers (1, 3, and 5) compared to the outermost layer (20). *STC1* and *CPA4* transcript levels appeared highest in the innermost layer that was in contact with *C. acnes*, whereas *ANGPTL4* and *NDNF* transcript levels appeared highest in layer 3 (**figure 4.6**). This finding may be reflective of either temporal gene expression regulation or *C. acnes*-induced cell death in the innermost layer.

Additionally, all four fibroblast genes exhibited significantly enhanced expression in SC fibroblasts from layers 1 to 3 when *C. acnes* was present in the S-JIM. This increase in gene expression was less significant in layer 5, and absent in layer 20 (the outermost layer), presumably due to the absence of *C. acnes* at the higher oxygen levels. While the present data cannot confirm whether direct or indirect contact with *C. acnes* was responsible for these gene expression changes, it does illustrate all four putative biomarkers were upregulated by the presence of *C. acnes* in the S-JIM, consistent with the RNA sequencing analyses in the FBCC model.

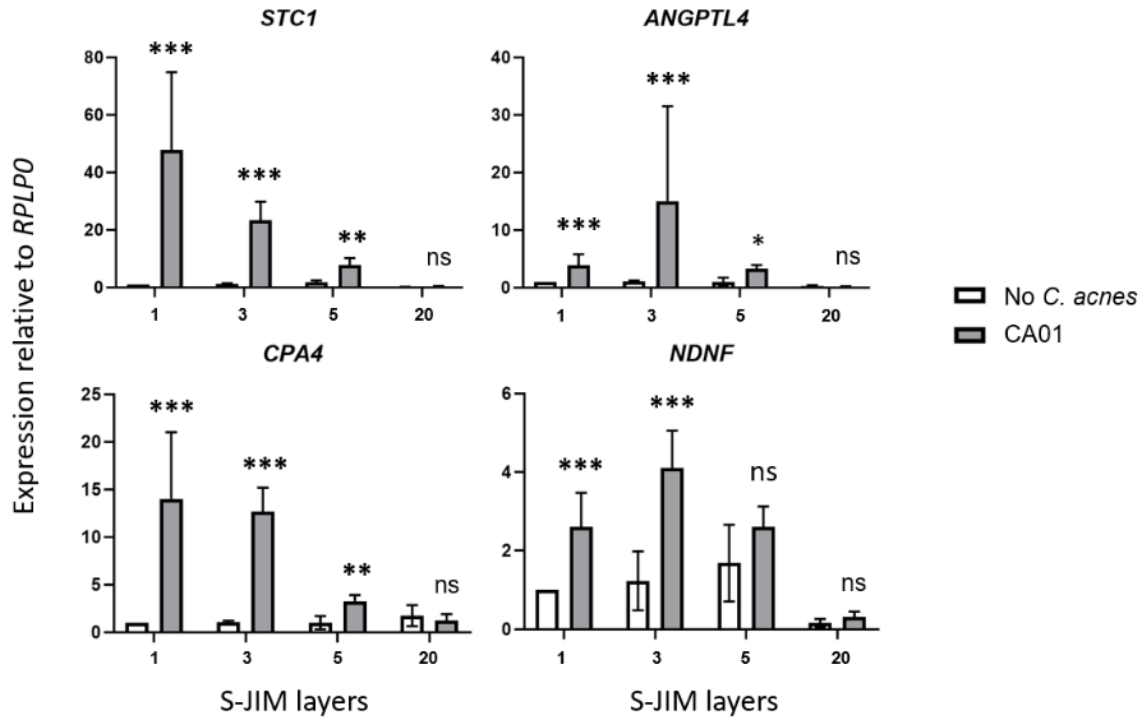


Figure 4.6. Putative SC Fibroblast Biomarker Gene Expression Changes in Response to *C. acnes* in the S-JIM.

S-JIMs were set up according to the optimized protocol (**methods 2.3**). Relative mRNA levels in S-JIM layers 1 (innermost), 3, 5, and 20 were assessed by real time PCR and normalized to *RPLP0*. All experiments were performed in triplicates (n = 3). *STC1*, *Stanniocalcin-1*; *ANGPTL4*, *Angiopoietin-like 4*; *CPA4*, *Carboxypeptidase A4*; *NDNF*, *Neuron derived neurotrophic factor*. Error bars indicate 95% confidence interval range. Significant differences in gene expression between the CA01 condition and no *C. acnes* control was calculated independently for each S-JIM layer. * p < 0.05, ** p < 0.01, *** p < 0.001

4.7 Applications of the Shoulder-Joint Implant Mimetic

4.7.1 Overview

Given that the S-JIM is a newly developed model, it was necessary to confirm its reproducibility and preclinical validity. Two studies related to the detection and prevention of *C. acnes*-associated shoulder PJIs were selected for investigation using the S-JIM.

1. Evaluating the prophylactic benefit of vancomycin treatment against *C. acnes* during shoulder arthroplasty.
2. Confirming the prospective use of desorption electrospray ionization mass spectrometry as a point-of-care diagnostic assay for *C. acnes* PJIs.

4.7.2 Validation of Vancomycin Prophylaxis in *C. acnes* PJI

Vancomycin is often considered a first-choice drug for postoperative infection in orthopedics as it is effective against commonly-encountered staphylococci species.⁹² However, the clinical benefit of using vancomycin in *C. acnes*-associated shoulder PJIs is currently unclear, as the number of PJI patients in most hospitals is generally too low to provide statistically significant data. The cost of vancomycin is not a prohibitive factor⁹³, but a prolonged trough serum concentration above 15 – 20 µg/mL can increase the risk of renal function deterioration.¹⁹ The goal of this study was to evaluate the bactericidal effectiveness of vancomycin treatment against *C. acnes* in the S-JIM model.

The first step was to assess the functional activity of vancomycin in the presence of human fibroblasts, as it was unclear whether these cells could clear, degrade, or chemically alter the antibiotic. To do so, changes in vancomycin concentration were extrapolated from disc diffusion assays following incubation with SC fibroblasts, as described in **figure 4.7A**. There was no statistical difference between the zones of inhibition radii of vancomycin that was incubated with SC fibroblasts (blue line) and vancomycin incubated without SC fibroblasts (orange line) after 48 hours (**figure 4.7B**). This pattern was consistent across a range of initial vancomycin concentrations (0 to 500

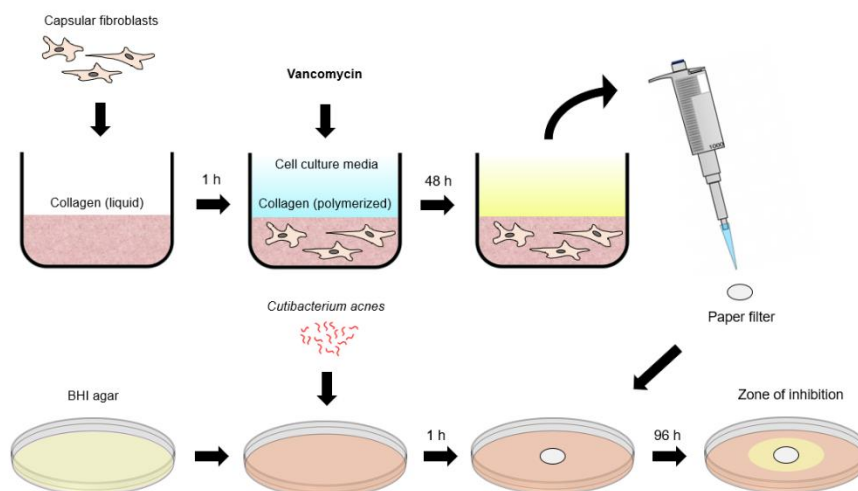
µg/mL), which indicated that vancomycin degradation was not enhanced by the presence of SC fibroblasts during the first 48 hours.

Having established that SC fibroblasts do not degrade vancomycin under these *in vitro* conditions, the next step was to model clinical vancomycin delivery using the S-JIM. For the purpose of preventing orthopedic infections, vancomycin can either be applied directly to the surgical site as a powder or injected into circulation. The direct intrawound application of vancomycin was modelled in the S-JIM by smearing vancomycin powder directly onto the innermost layer (embedded with *C. acnes*) at a surface coverage of 7.4×10^2 mg/mm². The intravenous delivery of vancomycin was modelled by dissolving vancomycin powder in the S-JIM culture media. Media vancomycin concentrations of 5 µg/mL to 20 µg/mL were selected for this experiment, representing the clinical consensus for the lower and upper limits of effective trough serum concentrations for infection prophylaxis in the average adult.^{81,82}

To assess *C. acnes* survival following the two approaches of vancomycin application in the S-JIM, the innermost strip was removed after 48 hours of co-culture, washed briefly in fresh cell culture media, and a 100 µL aliquot of this media was plated onto BHI agar. Resulting colony counts correlated with the relative survival of *C. acnes* after co-culture in the S-JIM model. There were no significant differences in colony counts between the two *C. acnes* strains across experimental conditions. *C. acnes* colonies consistently appeared in all replicates when vancomycin was absent in either the S-JIM or the culture media, indicative of *C. acnes* survival following co-culture in the S-JIM. In contrast, no *C. acnes* colonies were observed when vancomycin was applied directly as a powder or dissolved in DMEM-soy at a concentration of 20 µg/mL. However, at a lower vancomycin concentration of 5 µg/mL, *C. acnes* colonies were observed in half of the experimental replicates. The average colony count at this reduced vancomycin concentration was fewer than the one presented in the no vancomycin condition (22 vs 705 CFU/mL), which suggests that vancomycin was effective at reducing *C. acnes* survival in the S-JIM but did not completely eradicate the bacteria in half of the replicates (**Table 4.2**). These results indicate that vancomycin was effective against *C. acnes* when

applied directly as a powder and dissolved in media at a sufficiently high concentration, but routine intravenous delivery may fall below this effective concentration.

A



B

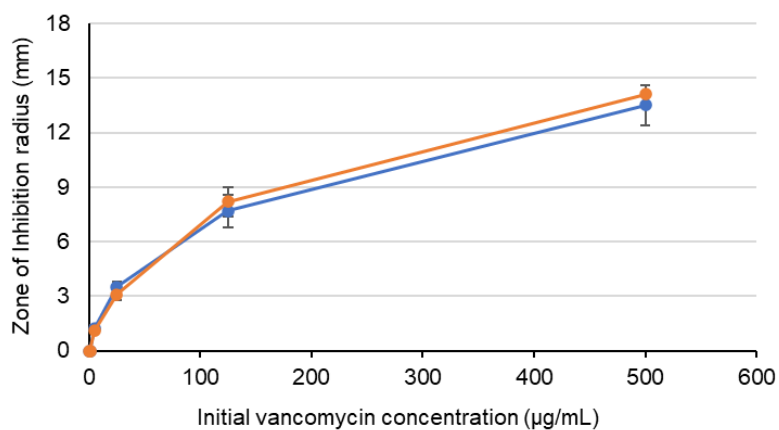


Figure 4.7. SC fibroblasts do not alter vancomycin degradation rate.

SC fibroblasts were cultured in 3D collagen as described in the FBCC model (**methods 2.2**). Vancomycin hydrochloride powder was dissolved in cell culture media and incubated with SC fibroblasts for 48 hours. A 50 µL aliquot of this media was pipetted onto a paper filter and positioned in the center of a BHI agar plate evenly spread with *C. acnes*. Agar plates were incubated anaerobically (0% O₂, 5% CO₂, 37° C) for 96 hours to allow for *C. acnes* growth. Radii of zones inhibitory to *C. acnes* growth were measured and correlated to the initial vancomycin concentrations. **(B)** Zones of inhibition are shown for vancomycin-containing cell culture media following incubation with SC fibroblasts. Blue and orange lines represent dataset with and without SC fibroblasts, respectively. There were no significant differences in vancomycin degradation between samples cultured in the presence and absence of SC fibroblasts. All experiments were performed in triplicate (N = 3).

Table 4.2. *C. acnes* survival following vancomycin application in the S-JIM (n = 3).

SC fibroblast culture	<i>C. acnes</i> strain	<i>C. acnes</i> colony forming units (CFU/100 μ L)			
		No vancomycin	Vancomycin powder	Media vancomycin 20 μ g/mL	Media vancomycin 5 μ g/mL
SC 1	11827	92	0	0	9
SC 1	PA01	50	0	0	0
SC 2	11827	28	0	0	0
SC 2	PA01	93	0	0	1
SC 3	11827	100	0	0	0
SC 3	PA01	60	0	0	3

4.7.3 Detecting *C. acnes* PJI by Desorption Electrospray Ionization Mass Spectrometry

As previously mentioned, the ideal diagnostic approach for *C. acnes* PJI would be a point-of-care assay that can provide a rapid diagnosis while the patient is on the operating table. The iKnife is a newly developed surgical tool that may allow surgeons to accomplish this by scanning for microbe-specific molecular markers in periprosthetic tissues during an operation. In brief, the iKnife functions by sublimating a region of tissue, creating a gaseous sample that is subsequently analyzed by rapid evaporative ionization mass spectrometry.⁹⁴ This suggests that the iKnife may be capable of differentiating between healthy tissues and *C. acnes*-infected tissues. However, it is currently unclear whether *C. acnes* biomarkers are detectable in connective tissues using mass spectrometry.

The S-JIM model was used to provide proof-of-concept for the use of mass spectrometry in detecting a *C. acnes* PJI. In brief, S-JIM strips mimicking connective tissues were embedded with collagen or collagen with SC fibroblasts and coated with *C. acnes* CA01. The strip surface was then scanned using DESI-MS, and relative m/z signal intensities were translated into a representative 2D field-of-view image. Each pixel represents a DESI-MS datapoint correlating to an individual physical location on the S-JIM strip. Relative signal intensities were generated for a full m/z spectrum of 100 to 1000 for each pixel. The field-of-view images resulting from the relative signal intensities at $m/z = 377$ and $m/z = 473$ are shown in **figure 4.8**.

The identities of the $m/z = 377$ and $m/z = 473$ ions are unknown, but the data suggests they are specific to *C. acnes* and SC fibroblasts respectively. The images at $m/z = 377$ (**Figure 4.8A**) display high-intensity signals (yellow) corresponding to the regions where *C. acnes* was smeared on the surface. Conversely, at $m/z = 473$ (**Figure 4.8B**), the high-intensity signals were no longer present. Rather, these imaged regions were entirely uniform in low-intensity signals (blue). There were however high intensity signals corresponding to the S-JIM strip embedded with SC fibroblasts. These data indicate the possibility of independently identifying the presence and location of SC fibroblasts and *C. acnes* within a PJI using DESI-MS.

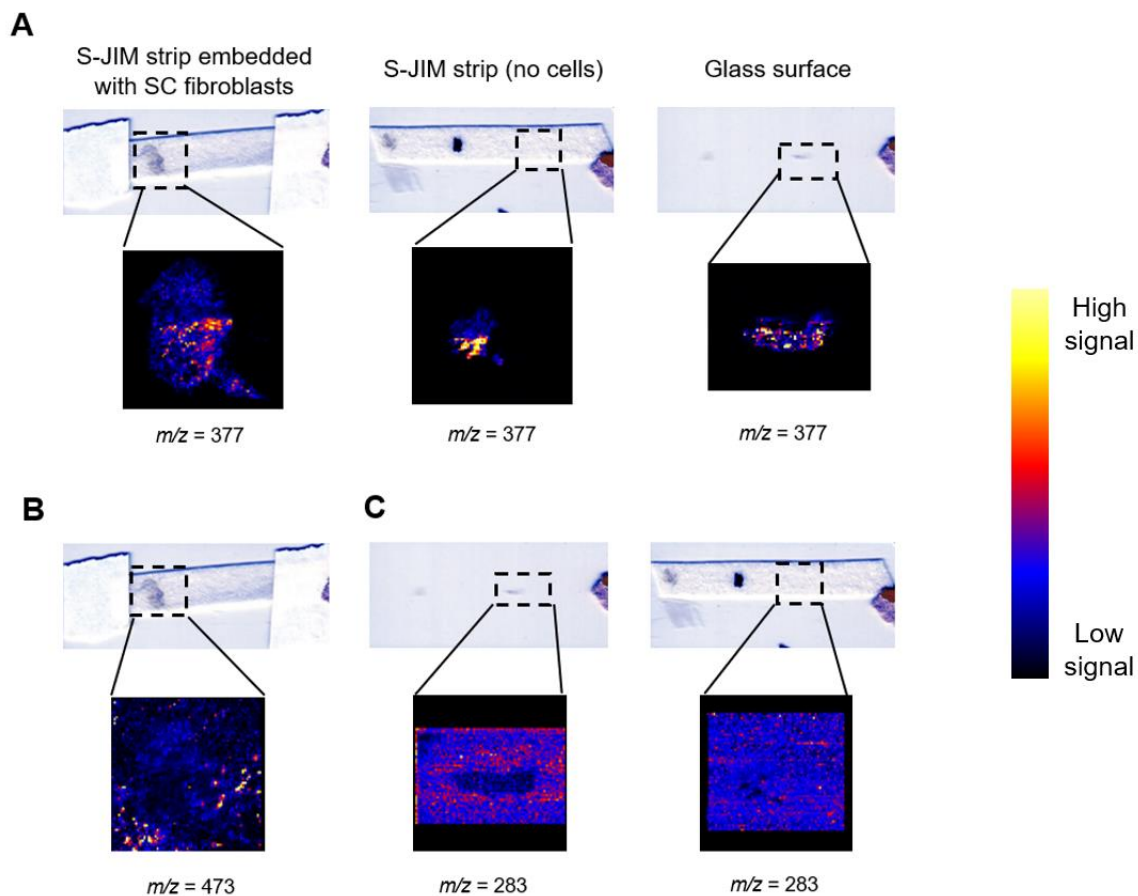


Figure 4.8. Detection of Ions Specific to *C. acnes* and SC fibroblast in S-JIM strips.

Surfaces of glass microscope slides, S-JIM strips embedded with collagen and without cells, and S-JIM strips embedded with collagen and SC fibroblasts were coated with *C. acnes* and scanned using Desorption Electrospray Ionization Mass Spectrometry (**methods 2.4**). Raw desorption data was translated into 2D field-of-view images for ions with (**A**) $m/z = 377$, (**B**) $m/z = 473$, and (**C**) $m/z = 283$. Signal intensity is displayed as follows: blue (low), red (medium) and yellow (high). All DESI-MS handling and analyses were performed by the Zarrine-Afsar lab from the University Health Network, Toronto, Canada.

Chapter 5

5 Shoulder-Joint Implant Mimetic (S-JIM)

5.1 *C. acnes* Induces a Pro-Inflammatory Response in SC Fibroblasts

Quantitative PCR analyses of SC fibroblasts gene expression in the FBCC model (**figure 3.3**) indicated an overall pro-inflammatory response following co-culture with *C. acnes*. This was expected, as inflammation is an established hallmark of microbial joint infection.⁹⁵ Additionally, consistent with our findings, *C. acnes* has been previously shown to secrete porphyrins, most commonly coproporphyrin III, that cause inflammation by generating reactive oxygen species.⁹⁶ *C. acnes* can also express and secrete CAMP factor during an acne outbreak, which initiates an inflammatory response by causing the cell death of sebocytes in sebaceous glands.⁹⁷ However, it is interesting to note that despite strong evidence suggesting that *C. acnes* induces host tissue inflammation, common serum inflammatory biomarkers such as C-reactive proteins, erythrocyte sedimentation rate, and white blood cell counts are oftentimes reportedly unchanged throughout a *C. acnes* infection.^{58,59} This apparent discrepancy between local and systemic responses to inflammation may be indicative of inefficient endocrine signaling at the site of infection, likely due to the poor vascularity of the dense connective tissues lining the post-operative shoulder joint.

Of the five inflammatory cytokines that were observed, *IL-6*, *TNF*, and *CCL2* gene expression levels were significantly different between SC fibroblasts that were co-cultured with *C. acnes* for 24 and 48 hours (**figure 3.3**). *IL-6* (*Interleukin 6*) is a central pleiotropic cytokine that functions as the chief stimulator for the production of most plasma proteins involved in acute inflammation.^{85,86} Given its important role in promoting inflammation, it is unsurprisingly that its gene expression was significantly upregulated 3 to 4-fold in SC fibroblasts after 24 hours of co-culture with *C. acnes*. The return of *IL-6* gene expression to pre-infection levels after 48 hours of co-culture appears counterintuitive but may be attributed to a global repression of cellular processes – and thereby gene expression activity – in response to microbial infection. This hypothesis is

supported by the fact that 77% of the 4889 SC fibroblast genes with significantly altered expression activity were downregulated following exposure to *C. acnes* (**figure 3.6**). Furthermore, 20 of the 22 significantly enriched cellular pathways derived from RNA sequencing analysis (**table S1**) were also downregulated.

A second explanation may be the presence of a negative feedback loop that serves to inhibit prolonged IL-6 production and prevent inflammatory tissue damage. One such self-regulatory pathway was recently discovered by Verboogen *et al.*, in which newly synthesized IL-6 molecules bound to endosomal receptors while in transit to the plasma membrane.⁸⁵ This activity resulted in the phosphorylation of STAT3 (Signal Transducer And Activator Of Transcription 3), which subsequently repressed the gene expression of *IL-6*. While it is not possible to determine the validity of these explanations based on the present data, our experiment does highlight the time-sensitive nature of *IL-6* gene expression. Therefore, in consideration of recent studies that have proposed IL-6 as a biomarker of shoulder infection,^{98,99} it is advisable to remain cautionary in using this cytokine to diagnose PJI.

Similar to *IL-6*, *TNF* is a pro-inflammatory cytokine that coordinates a subset of plasma proteins involved in acute inflammation.^{86,87} Interestingly, *TNF* gene expression was unchanged in SC fibroblasts after 24 hours of co-culture with *C. acnes*, but significantly upregulated after 48 hours. This was completely contrary to the gene expression activity of *IL-6* after 24 and 48 hours of co-culture. However, the result was expected, as *TNF* is one of the many pro-inflammatory regulated by *IL-6* following prolonged exposure to microbial endotoxins.⁸⁸ The increased gene expression of *IL-6* after 24 hours was likely responsible for repressing *TNF* gene expression. It is also important to note that *IL-6* reportedly does not regulate anti-inflammatory cytokines⁸⁸, which explains why *IL-10* gene expression levels were consistent after 24 and 48 hours of co-culture.

The *TNF* and *IL-17* pro-inflammatory signaling pathways (**figure S1**) were the only two cellular pathways that were enriched by the RNA sequencing analyses but did not reflect an overall decrease in gene expression. Although more of the genes in these two pathways were downregulated than upregulated, it is interesting to note that most of the

upregulated genes in these pathways were downstream transcriptional targets, whereas most of the downregulated genes encoded early signaling molecules such as transcription factors. These results are consistent with our previous observations of the temporal regulation in cytokine gene expression (**figure 3.3**) and further support the existence of a negative feedback mechanism that inhibits the inflammation signaling cascade after the final gene products have been generated.

5.2 Limitations of the FBCC Model

The FBCC model provided a reliable system to rapidly assess the impact of *C. acnes* on the gene expression of SC fibroblasts under hypoxic (2% O₂) conditions that are characteristic of the shoulder joint. In theory, it was also possible to assess the impact of SC fibroblasts on the gene expression of *C. acnes* using the same RNA sequencing dataset. This was our initial goal, however the percentage of microbial transcripts in the extracted RNA pool was too low and provided an insufficient read count for genome alignment. It was later determined that this was likely because our RNA extraction protocol (Direct-zol RNA MiniPrep kit from Zymoresearch) did not include a sufficient Trizol incubation period to fully dissolve the peptidoglycan in *C. acnes* cell walls, resulting in underrepresentation of microbial RNA in the extraction. Fortunately, most of the microbial RNA in the samples could be filtered from the raw data and ultimately did not interfere with downstream analyses of the SC fibroblasts transcriptomic profile.

The FBCC model, while efficient, is limited in its content validity and range of possible data collection methods. First, the FBCC model only provided a constant 2% O₂ environment rather than the dynamic range of oxygen levels present in the different layers of shoulder connective tissue. Second, the FBCC model did not consist of an implant surface, which was reportedly necessary for microbial growth in mice models of PJI.⁵² Third, it was not possible to assess gene expression changes or directly image cells at different layers of the fragile collagen disc due to a lack of a scaffolding framework. Fourth, the FBCC model can only capture gene expression changes from the entire population of SC fibroblast and *C. acnes* cells, but not cells at specific locations and distances apart. These limitations suggest that the gene expression analyses derived from the FBCC model may not accurately represent the actual gene expression changes in SC

fibroblasts *in vivo*. The S-JIM model was designed to address these four limitations and provide superior content validity for future experiments.

5.3 Potential Improvements to the S-JIM Model

The results in this thesis highlight the development of the first 3D laboratory biomimetic of an artificial human shoulder joint. While the S-JIM provides several advantages over 2D cell cultures for studying PJI, such as the presence of an implant surface and the generation of a physiologically representative oxygen gradient across tissue layers (**figure 4.2**), there are some limitations to the model design. For example, the S-JIM is a stationary model and does not articulate like a functional shoulder joint. Consequently, there would be a lack of periodic fluid circulation, which would naturally be present in a post-operative synovial joint cavity.¹⁰⁰ The absence of fluid flow would likely hinder *C. acnes* migration in the S-JIM, as it lacks the cellular structures required for autonomous motility.⁴¹ This limitation could be mitigated by culturing the S-JIM on a shaker that is periodically controlled, although this could compromise the setup needed to achieve anaerobic conditions.

The S-JIM was developed as a co-culture system, but the only human cell type included in the current model is the SC fibroblast. While it is impractical to aim for a complete cellular representation of capsular connective tissue within a single model, the addition of circulating immune cells would be beneficial given the context of infection. As indicated by the gene expression analyses of SC fibroblasts from the FBCC model, the pro-inflammatory TNF and IL-17 signaling pathways were activated by the presence of *C. acnes* but remained unresolved after 48 hours (**figures 3.3 and S1**) due to the lack of an immune response. One method of replicating the immune response in the S-JIM could involve supplementing the cell culture media with the buffy coat of a patient blood sample (i.e. a concentration of all the white blood cells and platelets). Alternatively, introducing THP-1 monocytes (an immortalized cell line routinely used for *in vitro* studies) at the outermost layer of the S-JIM could mimic the physiological process whereby monocytes transform into macrophages and migrate through the tissue layers in response to pro-inflammatory cytokines. This latter approach would provide less experimental validity, but presumably allows easier assessment of cellular responses

given the lower number of total cell types in the S-JIM. These putative improvements to the S-JIM model would allow us to investigate if the adaptive immune response can effectively clear early *C. acnes* infections, or whether the infection can achieve a critical mass in time to evade the host immune response.

Another important consideration is that the S-JIM may not represent the actual number of *C. acnes* cells present throughout the stages of an *in vivo* PJI. Infection in patients likely initiates at the site(s) of contamination and gradually propagates across the implant. In the S-JIM, *C. acnes* was instead evenly distributed in the strip at a concentration of 5.0×10^6 cells/mL of collagen, resulting in a bacterial count that is presumably greater than the amount present in an *in vivo* PJI. A more physiologically representative *C. acnes* count was not replicated in the S-JIM model in order to ensure that an *in vitro* PJI could be generated within a reasonable timespan (2 to 4 days) as opposed to the several weeks to months of lag time that often precedes the clinical onset of PJI.⁷ As such, the detection of *C. acnes* biomarkers from the DESI-MS scan may portray an overly-optimistic view of the ability to detect *C. acnes* in patient tissues. Conversely, the clinical effectiveness of intravenous vancomycin prophylaxis may be greater than the data presented in this thesis given the lower quantity of *C. acnes* that would need to be eradicated in patient tissues. Future S-JIM experiments seeking a more realistic temporal representation of the infection process should either lower the initial *C. acnes* concentration or apply *C. acnes* at a single point on the implant surface, allowing the infection to develop across the implant surface.

5.4 SC Cell Death in the Presence of *C. acnes*

The SC fibroblasts were viable at all oxygen levels tested in the S-JIM when cultured in the absence of *C. acnes* (**figure 4.3**). This is an important distinction between the S-JIM and the TRACER model that the S-JIM was cross-purposed from. In TRACER, cells were viable in the oxygen-abundant outer strip layers, but the majority were non-viable near the hypoxic core.⁹⁰ We hypothesize this is because the SKOV3 and MCF7 tumor cell lines used in TRACER exhibit greater metabolic activity, and thereby an increased rate of oxygen consumption, compared to non-cancerous cells in homeostasis. In contrast, the SC fibroblasts used in the S-JIM exhibit a low metabolic rate *in vivo* and have

correspondingly low oxygen requirements, presumably as an adaptation to the low oxygen environment of a normal joint capsule.

The cellular lysis of SC fibroblasts observed in response to co-culture with *C. acnes* in the S-JIM is consistent with clinical reports of tissue necrosis in PJI.²¹ While the molecular mechanisms by which *C. acnes* induces cell lysis in a PJI is unclear, the live-dead cell assay (**figure 4.3**) suggests that the microbial influence was localized to the innermost layers that were in physical contact with *C. acnes*. This suggests that *C. acnes* cells in the S-JIM did not migrate from their initial site of culture, consistent with the nature of *C. acnes* as a non-motile microorganism.⁴¹ Accordingly, the direct intrawound application of antimicrobial powders as a surgical prophylaxis would predictably be effective against *C. acnes* PJI, as it targets the initial site that *C. acnes* would adhere to.

5.5 Bactericidal Efficiency of Vancomycin Against *C. acnes* in the S-JIM.

The application of vancomycin powder in the S-JIM effectively eliminated both the repository skin-derived (ATCC 11827) and deep tissue-derived (CA01) *C. acnes* strains across all experimental replicates (**table 4.2**), which reinforces direct intrawound delivery of vancomycin as an effective clinical prophylaxis against *C. acnes* in shoulder PJI.

Vancomycin also eliminated *C. acnes* in the S-JIM when dissolved at 20 µg/ml in the media. However, when this concentration was reduced to 5 µg/ml, there were observations of *C. acnes* survival in some experimental replicates despite the fact that this concentration was ten times higher than vancomycin's previously reported minimal inhibitory concentration ($MIC_{50} = 0.38 \mu\text{g/ml}$ and $MIC_{90} = 0.5 \mu\text{g/ml}$).⁹² One explanation for this discrepancy might be inefficient vancomycin diffusion across the S-JIM layers, designed to mimic the connective tissue surrounding an avascular prosthetic joint. The thickness and permeability of the S-JIM layers may not be directly comparable to that of shoulder connective tissue, but it is noteworthy that collagen, the protein that constitutes the extracellular matrix in the S-JIM, represents most of the dry weight composition in connective tissues (60% in articular cartilage, 80% in joint ligaments, and 70% in tendons).¹⁰¹⁻¹⁰³ This suggests there is at least a similar degree of permeability between

extracellular matrices of the S-JIM and capsular tissues from a structural perspective. The S-JIM data therefore highlights the potential for physiological barriers in the shoulder to limit vancomycin administration to an avascular prosthesis in sufficient concentrations to prevent infection. Long-term intravenous administration of vancomycin may reduce *C. acnes* numbers in a PJI to aid the host immune response but is unlikely to be as effective as direct intrawound application.

The drawback to these experiments is that the toxicity of vancomycin on host fibroblasts was not thoroughly explored. While vancomycin would not be expected to act on fibroblasts given that its mode of action involves blocking the synthesis of peptidoglycan cell walls, long-term exposure (48 h) to a vancomycin concentration above 3 mg/cm² has been reported to be significantly cytotoxic to fibroblasts.¹⁰⁴ Furthermore, there have been reports of increased operative complications and prolonged wound healing associated with intrawound vancomycin delivery in knee arthroplasty patients.¹⁰⁵ Fortunately, intrawound delivery of vancomycin has also been reported to yield effective therapeutic levels within post-operative knee and hip joints while systemic vancomycin concentrations remain at subtherapeutic or even undetectable levels.¹⁰⁶ The fibroblasts used in our experiments did not show any phenotypes indicative of cell lysis when observed under a light microscope (data not shown) but they were not observed beyond 24 hours. The potential for long term detrimental effects of vancomycin powder application on shoulder connective tissue cell viability cannot be ruled out without additional and much more comprehensive analyses.

5.6 Explanations for the Lack of Biofilm Formation in the S-JIM

The SEM images (**figure 4.4**) revealed that while individual *C. acnes* cells adhered to the S-JIM implant surface, extracellular polymeric substances that are characteristic of *C. acnes* biofilms⁴⁵ were not detected. This contrasts with previous studies of *C. acnes* PJIs.^{21,46,58,107} However, while biofilm formation is generally regarded as a hallmark of *C. acnes* PJI, it is noteworthy that no studies so far, to the best of our knowledge, have directly imaged *C. acnes* biofilms from an infected implant that has been extracted from a patient. It is, therefore, possible that *C. acnes* may not form the typical biofilm matrices

that are routinely observed *in vitro* within the environment of an infected human joint. This hypothesis is consistent with the observation that biofilms do not appear to be essential for at least some of the infectious properties of *C. acnes*. For example, as the cell viability assays (**figure 4.3**) and SEM images (**figure 4.4**) demonstrate, the ability of *C. acnes* to engender cell lysis in adjacent fibroblasts and adhere to the implant surface occurred in the absence of biofilms. Confirming the *in vivo* *C. acnes* biofilm structure would be a critical next step in determining whether the absence of biofilms in the S-JIM is physiologically representative or a limitation in the model.

From the follow-up experiments exploring *in vitro* *C. acnes* biofilm formation on horizontal surfaces, it was evident that changes to media concentration (**figure 4.5B**), serum concentration (**figure 4.5C**), or surface roughness (**figure 4.5D**) were ineffective in converting *C. acnes* from a planktonic to biofilm mode of growth. Interestingly, the only method that succeeded in promoting *C. acnes* biofilm formation was changing the DMEM-soy co-culture media we developed back to BHI, one of the routine microbial growth medias for culturing *C. acnes* (**figure 4.5A**). Comparatively, DMEM does not contain a lipid metabolic source whereas BHI presumably does as it is comprised largely of cow brain extract.¹⁰⁸ These lipids are generally serve as component building blocks for microbial biofilms¹⁰⁹ and may be necessary act as a signal *C. acnes* biofilm formation, given that the bacteria naturally forms biofilms in the lipid-rich sebaceous glands.³⁴ Regardless of the specific factor(s) that enabled *C. acnes* biofilm formation in BHI but not DMEM, the result could not be replicated in the S-JIM with BHI, which indicates there is another factor hindering *C. acnes* biofilm formation.

The biophysical mechanisms underlying microbial biofilm development aids in explaining the discrepancies in *C. acnes* biofilm formation between 2D culturing conditions and the S-JIM. During the initial stages of biofilm formation, rod-shaped bacteria under 10 μm in length have been experimentally shown to aggregate into a 3D cluster of radially-aligned cells that are vertically-aligned to the surface (**figure 5.1**).¹¹⁰ The transition of cells from a horizontal to vertical orientation is driven by localized mechanical instabilities caused by the lengthening and division of neighboring cells.

Given that radial length of *C. acnes* is between 3 to 5 μm ,¹¹¹ the initiation of its biofilm likely adopts the same pattern.

The role of this 3D conformation is not currently understood, but one possible function could be to increase the local cell density. This is achieved by the vertical side-by-side packing of cells, which would allow more cells to occupy a given surface area compared to if they were radially-aligned with the surface. Importantly, once *C. acnes* reaches a critical cell density, the bacteria undergoes quorum sensing and begins to secrete autoinducer AI-2.⁴⁶ This molecule subsequently triggers a signaling cascade that results in the upregulation of several genes involved in biofilm formation. It is therefore tempting to speculate that the formation of this 3D conformation is at least partially responsible for triggering the expression of quorum signals that enable *C. acnes* to transition from a planktonic to biofilm mode of growth.

If this hypothesis is correct, then *C. acnes* in the S-JIM may not have entered the biofilm mode of growth because such a conformation would be unlikely to form on a vertically orientated implant surface. This is because *C. acnes* has been observed to sediment in a stationary culture (data not shown), and cells that align perpendicular with the vertical surface may lack the surface contact required for adherence to the implant. This explanation would be consistent with our experiments wherein *C. acnes* biofilms formed on horizontal surfaces but not on the vertically oriented S-JIM surface. It may therefore be more appropriate to culture the S-JIM in the horizontal orientation as opposed to the vertical orientation.

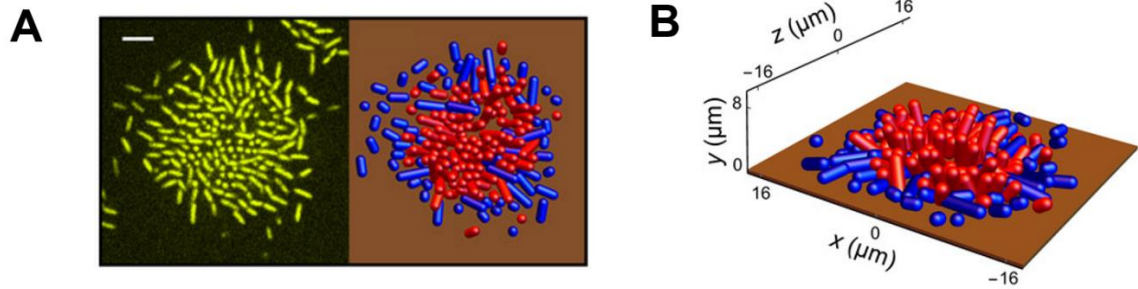


Figure 5.1. 3D Microbial Clustering During Biofilm Initiation. (A) Top-down and (B) side view of microbial biofilm initiation after transformation into a computer model. Vertically and horizontally aligned cells are labelled red and blue, respectively. Images adapted from Beroz et al (2018).

5.7 Prospective Real-Time Detection of *C. acnes* PJIs Using Mass Spectrometry

The DESI-MS experiments highlighted the use of a *C. acnes*-specific molecular ion to detect regions of “infected” bioartificial tissue. The identity of this molecular ion was not confirmed in this thesis, as the experiments only served to provide proof-of-concept, and more specific ions have been previously reported. For example, Teramoto *et al.*, demonstrated that matrix-assisted laser desorption/ionization mass spectrometry analyses of ribosomal subunit proteins to not only detect *C. acnes*, but also to classify individual strains into the six main phylotypes.¹¹² The ability to identify *C. acnes* strains beyond the species level suggests that mass spectrometry approaches engender sufficient specificity for the clinical detection of *C. acnes* in PJIs.

Adoption of mass spectrometry-based detection approaches could potentially be realized by using the novel iKnife™ – a handheld diathermy device that sublimates a selected region of tissue and immediately processes it using rapid evaporative ionization mass spectrometry (REIMS).⁹⁴ The molecular ions that are detected from the tissue sample are subsequently screened against a set of standard molecular markers based on their m/z ratios to characterize the sample. This process would allow surgeons to rapidly differentiate between “infected” and “non-infected” connective tissue during an operation. While the iKnife™ has so far only been used intraoperatively to assess *in vivo* tissues such as brain tumors^{113,114} and colorectal mucosa,¹¹⁵ its adoption for detecting microbial infections in patient tissue remains an unexplored but feasible possibility.

Further experiments would need to be conducted using the S-JIM before clinical testing is possible. In this thesis, DESI-MS was used in place of REIMS due to ease of accessibility. However, given that REIMS involves a more destructive sample analysis approach compared to DESI-MS,¹¹⁶ it is unclear if the same experimental outcomes would result. Furthermore, to rule out the possibility of cross-microbial detection, the selected molecular ions must be tested against other common agents involved in shoulder PJI, such as *Staphylococcus aureus*. Despite these limitations, the present data has provided an optimistic proof-of-concept view for the real-time detection of *C. acnes* PJIs using mass spectrometry.

5.8 Conclusion

To our knowledge, the S-JIM is the first *in vitro* 3D model of PJI that includes surgical metals and supports a co-culture of anaerobic bacteria and human capsular fibroblasts. The S-JIM provides substantial advantages over existing animal models and 2D cell culture systems for studying PJI, such as a physiologically accurate oxygen gradient and the ability to assess cellular and molecular interactions at several tissue layers. These data demonstrate the practicality of using the S-JIM to successfully address clinical inquiries such as the effectiveness of vancomycin prophylaxis and the prospective use of mass spectrometry as a point-of-care approach to detect *C. acnes* infections. While it is currently unclear whether *C. acnes* biofilms form *in vivo*, the S-JIM nevertheless has potential to serve as a valuable preclinical tool for studying the early stages of PJI.

References

1. Namba, R. S., Inacio, M. C. S. & Paxton, E. W. Risk factors associated with deep surgical site infections after primary total knee arthroplasty: An analysis of 56,216 knees. *J. Bone Jt. Surg. - Ser. A* (2013) doi:10.2106/JBJS.L.00211.
2. Edwards, J. R. *et al.* National Healthcare Safety Network (NHSN) report: Data summary for 2006 through 2008, issued December 2009. *Am. J. Infect. Control* (2009) doi:10.1016/j.ajic.2009.10.001.
3. Prosthetic joint infection: Epidemiology, microbiology, clinical manifestations, and diagnosis - UpToDate. <https://www.uptodate.com/contents/prosthetic-joint-infection-epidemiology-microbiology-clinical-manifestations-and-diagnosis/print>.
4. Carreau, A., Hafny-Rahbi, B. El, Matejuk, A., Grillon, C. & Kieda, C. Why is the partial oxygen pressure of human tissues a crucial parameter? Small molecules and hypoxia. *J. Cell. Mol. Med.* **15**, 1239–1253 (2011).
5. Anderson, J. M., Rodriguez, A. & Chang, D. T. Foreign body reaction to biomaterials. *Seminars in Immunology* (2008) doi:10.1016/j.smim.2007.11.004.
6. Ulrich, S. D. *et al.* Total hip arthroplasties: What are the reasons for revision? *Int. Orthop.* (2008) doi:10.1007/s00264-007-0364-3.
7. Li, C., Renz, N. & Trampuz, A. Management of Periprosthetic Joint Infection. *Hip Pelvis* **30**, 138 (2018).
8. Parvizi, J., Adeli, B., Zmistowski, B., Restrepo, C. & Greenwald, A. S. Management of periprosthetic joint infection: The current knowledge - AAOS exhibit selection. *Journal of Bone and Joint Surgery - Series A* (2012) doi:10.2106/JBJS.K.01417.
9. Hernández-Vaquero, D. *et al.* Treatment of periprosthetic infections: An economic analysis. *The Scientific World Journal* (2013) doi:10.1155/2013/821650.
10. Bedair, H. *et al.* A History of Treated Periprosthetic Joint Infection Increases the Risk of Subsequent Different Site Infection. *Clin. Orthop. Relat. Res.* (2015) doi:10.1007/s11999-015-4174-4.
11. Kurtz, S. M., Lau, E., Watson, H., Schmier, J. K. & Parvizi, J. Economic burden of periprosthetic joint infection in the united states. *J. Arthroplasty* (2012) doi:10.1016/j.arth.2012.02.022.

12. Matsen, F. A. *et al.* Origin of propionibacterium in surgical wounds and evidence-based approach for culturing propionibacterium from surgical sites. *J. Bone Jt. Surg. - Ser. A* (2013) doi:10.2106/JBJS.L.01733.
13. Aggarwal, V. K., Rasouli, M. R. & Parvizi, J. Periprosthetic joint infection: Current concept. *Indian Journal of Orthopaedics* (2013) doi:10.4103/0019-5413.106884.
14. Kapadia, B. H. *et al.* Periprosthetic joint infection. *The Lancet* (2016) doi:10.1016/S0140-6736(14)61798-0.
15. Rodriguez-Merchan, E. C. Knee fusion or above-the-knee amputation after failed two-stage reimplantation total knee arthroplasty. *Archives of Bone and Joint Surgery* (2015) doi:10.22038/abjs.2015.4237.
16. Prendki, V. *et al.* Prolonged suppressive antibiotic therapy for prosthetic joint infection in the elderly: a national multicentre cohort study. *Eur. J. Clin. Microbiol. Infect. Dis.* (2017) doi:10.1007/s10096-017-2971-2.
17. Bakhsheshian, J., Dahdaleh, N. S., Lam, S. K., Savage, J. W. & Smith, Z. A. The use of vancomycin powder in modern spine surgery: Systematic review and meta-analysis of the clinical evidence. *World Neurosurgery* (2015) doi:10.1016/j.wneu.2014.12.033.
18. Kanj, W. W., Flynn, J. M., Spiegel, D. A., Dormans, J. P. & Baldwin, K. D. Vancomycin prophylaxis of surgical site infection in clean orthopedic surgery. *Orthopedics* (2013) doi:10.3928/01477447-20130122-10.
19. Rodvold, K. A. *et al.* Vancomycin pharmacokinetics in patients with various degrees of renal function. *Antimicrob. Agents Chemother.* (1988) doi:10.1128/AAC.32.6.848.
20. Tande, A. J. & Patel, R. Prosthetic joint infection. *Clin. Microbiol. Rev.* (2014) doi:10.1128/CMR.00111-13.
21. Izakovicova, P., Borens, O. & Trampuz, A. Periprosthetic joint infection: current concepts and outlook. *EFORT Open Rev.* (2019) doi:10.1302/2058-5241.4.180092.
22. Del Pozo, J. L. & Patel, R. Infection associated with prosthetic joints. *N. Engl. J. Med.* (2009) doi:10.1056/NEJMcp0905029.

23. JR, L. *et al.* Outcomes of Acute Hematogenous Periprosthetic Joint Infection in Total Ankle Arthroplasty Treated With Irrigation, Debridement, and Polyethylene Exchange. *Foot ankle Int.* **39**, 1266–1271 (2018).
24. Shoulder Joint Replacement - OrthoInfo - AAOS.
<https://orthoinfo.aaos.org/en/treatment/shoulder-joint-replacement/>.
25. Kadler, B. K., Mehta, S. S. & Funk, L. Propionibacterium acnes infection after shoulder surgery. *International Journal of Shoulder Surgery* (2015)
doi:10.4103/0973-6042.167957.
26. Arduino, J. M. *et al.* Staphylococcus aureus infections following knee and hip prosthesis insertion procedures. *Antimicrob. Resist. Infect. Control* (2015)
doi:10.1186/s13756-015-0057-4.
27. Achermann, Y., Goldstein, E. J. C., Coenye, T. & Shirtliff, M. E. Propionibacterium acnes: From Commensal to opportunistic biofilm-associated implant pathogen. *Clin. Microbiol. Rev.* (2014) doi:10.1128/CMR.00092-13.
28. Omer, H., McDowell, A. & Alexeyev, O. A. Understanding the role of Propionibacterium acnes in acne vulgaris: The critical importance of skin sampling methodologies. *Clin. Dermatol.* (2017) doi:10.1016/j.clindermatol.2016.10.003.
29. Castillo, D. E., Nanda, S. & Keri, J. E. Propionibacterium (Cutibacterium) acnes Bacteriophage Therapy in Acne: Current Evidence and Future Perspectives. *Dermatology and Therapy* (2019) doi:10.1007/s13555-018-0275-9.
30. Grice, E. A. *et al.* Topographical and temporal diversity of the human skin microbiome. *Science* (80-.). (2009) doi:10.1126/science.1171700.
31. Nazipi, S., Stødkilde, K., Scavenius, C. & Brüggemann, H. The Skin Bacterium Propionibacterium acnes Employs Two Variants of Hyaluronate Lyase with Distinct Properties. *Microorganisms* (2017) doi:10.3390/microorganisms5030057.
32. Dajnoki, Z. *et al.* Sebaceous Gland-Rich Skin Is Characterized by TSLP Expression and Distinct Immune Surveillance Which Is Disturbed in Rosacea. *J. Invest. Dermatol.* (2017) doi:10.1016/j.jid.2016.12.025.
33. Christensen, G. J. M. & Brüggemann, H. Bacterial skin commensals and their role as host guardians. *Benef. Microbes* **5**, 201–215 (2014).
34. Lee, Byun & Kim. Potential Role of the Microbiome in Acne: A Comprehensive

- Review. *J. Clin. Med.* (2019) doi:10.3390/jcm8070987.
35. Scholz, C. F. P. & Kilian, M. The natural history of cutaneous propionibacteria, and reclassification of selected species within the genus propionibacterium to the proposed novel genera acidipropionibacterium gen. Nov., cutibacterium gen. nov. and pseudopropionibacterium gen. nov. *Int. J. Syst. Evol. Microbiol.* (2016) doi:10.1099/ijsem.0.001367.
 36. Evans, C. A. & Mattern, K. L. The aerobic growth of Propionibacterium acnes in primary cultures from skin. *J. Invest. Dermatol.* (1979) doi:10.1111/1523-1747.ep12530309.
 37. Brzuszkiewicz, E. *et al.* Comparative genomics and transcriptomics of propionibacterium acnes. *PLoS One* (2011) doi:10.1371/journal.pone.0021581.
 38. Hall, G. S. *et al.* Growth curve for propionibacterium acnes. *Curr. Eye Res.* (1994) doi:10.3109/02713689408999875.
 39. Balgir, P. P., Dhiman, S. R. & Kaur, P. In silico prediction and qPCR validation of novel sRNAs in Propionibacterium acnes KPA171202. *J. Genet. Eng. Biotechnol.* (2016) doi:10.1016/j.jgeb.2016.03.002.
 40. Lood, R. & Collin, M. Characterization and genome sequencing of two Propionibacterium acnes phages displaying pseudolysogeny. *BMC Genomics* (2011) doi:10.1186/1471-2164-12-198.
 41. Mak, T. N. *et al.* Comparative genomics reveals distinct host-interacting traits of three major human-associated propionibacteria. *BMC Genomics* (2013) doi:10.1186/1471-2164-14-640.
 42. Mollerup, S. *et al.* Propionibacterium acnes: Disease-causing agent or common contaminant? detection in diverse patient samples by next- generation sequencing. *J. Clin. Microbiol.* **54**, 980–987 (2016).
 43. Qiu, B. *et al.* Cutibacterium acnes and the shoulder microbiome. *J. Shoulder Elb. Surg.* (2018) doi:10.1016/j.jse.2018.04.019.
 44. Syed, U. A. M. *et al.* Preoperative sterilization preparation of the shoulder: A comparative study evaluating gauze sponge and commercially available applicator prep stick. *Arch. Bone Jt. Surg.* (2018) doi:10.22038/abjs.2017.21767.1570.
 45. Holmberg, A. *et al.* Biofilm formation by Propionibacterium acnes is a

- characteristic of invasive isolates. *Clin. Microbiol. Infect.* (2009)
doi:10.1111/j.1469-0691.2009.02747.x.
46. Mooney, J. A. *et al.* Periprosthetic bacterial biofilm and quorum sensing. *Journal of Orthopaedic Research* (2018) doi:10.1002/jor.24019.
 47. Miller, M. B. & Bassler, B. L. Quorum Sensing in Bacteria. *Annu. Rev. Microbiol.* (2001) doi:10.1146/annurev.micro.55.1.165.
 48. O'Toole, G., Kaplan, H. B. & Kolter, R. Biofilm Formation as Microbial Development. *Annu. Rev. Microbiol.* **54**, 49–79 (2000).
 49. Del Pozo, J. L. Biofilm-related disease. *Expert Review of Anti-Infective Therapy* vol. 16 51–65 (2018).
 50. Platsidaki, E. & Dessinioti, C. Recent advances in understanding *Propionibacterium acnes* (*Cutibacterium acnes*) in acne [version 1; referees: 2 approved]. *F1000Research* (2018) doi:10.12688/f1000research.15659.1.
 51. Tabin, U. F., Corvec, S., Betrisey, B., Zimmerli, W. & Trampuz, A. Role of rifampin against *Propionibacterium acnes* biofilm in vitro and in an experimental foreign-body infection model. *Antimicrob. Agents Chemother.* (2012)
doi:10.1128/AAC.05552-11.
 52. Shiono, Y. *et al.* Delayed *Propionibacterium acnes* surgical site infections occur only in the presence of an implant. *Sci. Rep.* (2016) doi:10.1038/srep32758.
 53. Jokela, T. A. *et al.* Mannose reduces hyaluronan and leukocytes in wound granulation tissue and inhibits migration and hyaluronan-dependent monocyte binding. *Wound Repair Regen.* (2013) doi:10.1111/wrr.12022.
 54. Furustrand Tabin, U., Aubin, G. G., Eich, G., Trampuz, A. & Corvec, S. Occurrence and new mutations involved in rifampicin-resistant *Propionibacterium acnes* strains isolated from biofilm or device-related infections. *Anaerobe* (2015)
doi:10.1016/j.anaerobe.2015.05.003.
 55. Lo, C. W., Lai, Y. K., Liu, Y. T., Gallo, R. L. & Huang, C. M. *Staphylococcus aureus* Hijacks a skin commensal to intensify its virulence: Immunization targeting B-hemolysin and CAMP factor. *J. Invest. Dermatol.* (2011)
doi:10.1038/jid.2010.319.
 56. Wollenberg, M. S. *et al.* *Propionibacterium*-produced coproporphyrin III induces

- staphylococcus aureus aggregation and Biofilm formation. *MBio* (2014)
doi:10.1128/mBio.01286-14.
57. Tyner, H. & Patel, R. Hyaluronidase in Clinical Isolates of Propionibacterium acnes. *Int. J. Bacteriol.* (2015) doi:10.1155/2015/218918.
 58. Saper, D., Capiro, N., Ma, R. & Li, X. Management of Propionibacterium acnes infection after shoulder surgery. *Current Reviews in Musculoskeletal Medicine* (2015) doi:10.1007/s12178-014-9256-5.
 59. Portillo, M. E., Corvec, S., Borens, O. & Trampuz, A. Propionibacterium acnes: An underestimated pathogen in implant-associated infections. *BioMed Research International* (2013) doi:10.1155/2013/804391.
 60. Parvizi, J., Zmistowski, B. & Adeli, B. Periprosthetic joint infection: treatment options. *Orthopedics* (2010) doi:10.3928/01477447-20100722-42.
 61. Bossard, D. A. *et al.* Optimal length of cultivation time for isolation of Propionibacterium acnes in suspected bone and joint infections is more than 7 days. *J. Clin. Microbiol.* (2016) doi:10.1128/JCM.01435-16.
 62. Shields, M. V., Abdullah, L. & Namdari, S. The challenge of Propionibacterium acnes and revision shoulder arthroplasty: A review of current diagnostic options. *Journal of Shoulder and Elbow Surgery* (2016) doi:10.1016/j.jse.2016.01.009.
 63. SJ, F. *et al.* Early Versus Late Culture Growth of Propionibacterium acnes in Revision Shoulder Arthroplasty. *J. Bone Joint Surg. Am.* **97**, 1149–1158 (2015).
 64. Holmes, S., Pena Diaz, A. M., Athwal, G. S., Faber, K. J. & O’Gorman, D. B. Neer Award 2017: A rapid method for detecting Propionibacterium acnes in surgical biopsy specimens from the shoulder. *J. Shoulder Elb. Surg.* **26**, 179–185 (2017).
 65. Mortazavi, J. S. M. *et al.* Failure following revision total knee arthroplasty: Infection is the major cause. in *International Orthopaedics* (2011).
doi:10.1007/s00264-010-1134-1.
 66. Stavrakis, A. I., Niska, J. A., Loftin, A. H., Billi, F. & Bernthal, N. M. Understanding infection: A primer on animal models of periprosthetic joint infection. *The Scientific World Journal* (2013) doi:10.1155/2013/925906.
 67. Ahern, B. J., Richardson, D. W., Boston, R. C. & Schaer, T. P. Orthopedic

- Infections in Equine Long Bone Fractures and Arthrodeses Treated by Internal Fixation: 192 Cases (1990-2006). *Vet. Surg.* (2010) doi:10.1111/j.1532-950X.2010.00705.x.
68. Levy, N. The use of animal as models: Ethical considerations. *Int. J. Stroke* (2012) doi:10.1111/j.1747-4949.2012.00772.x.
69. Gahukamble, A. D. *et al.* Propionibacterium acnes and Staphylococcus lugdunensis cause pyogenic osteomyelitis in an intramedullary nail model in rabbits. *J. Clin. Microbiol.* (2014) doi:10.1128/JCM.03197-13.
70. Achermann, Y., Tran, B., Kang, M., Harro, J. M. & Shirliff, M. E. Immunoproteomic identification of in vivo-produced Propionibacterium acnes proteins in a rabbit biofilm infection model. *Clin. Vaccine Immunol.* (2015) doi:10.1128/CVI.00760-14.
71. Yen, T., Yuan, C.-Y. & Huang, C.-M. Current status of acne vaccines. *Expert Rev. Dermatol.* **5**, 561–567 (2010).
72. Perlman, R. L. Mouse Models of Human Disease: An Evolutionary Perspective. *Evol. Med. Public Heal.* (2016) doi:10.1093/emph/eow014.
73. Billings, L. Lab mice are too clean. *Scientific American* (2016) doi:10.1038/scientificamerican0716-12.
74. Bart van der Worp, H. *et al.* Can animal models of disease reliably inform human studies? *PLoS Med.* (2010) doi:10.1371/journal.pmed.1000245.
75. Hackam, D. G. & Redelmeier, D. A. Translation of research evidence from animals to humans [9]. *Journal of the American Medical Association* (2006) doi:10.1001/jama.296.14.1731.
76. Spittaels, K. J. & Coenye, T. Developing an in vitro artificial sebum model to study Propionibacterium acnes biofilms. *Anaerobe* (2018) doi:10.1016/j.anaerobe.2017.11.002.
77. Aubin, G. G. *et al.* Interaction of Cutibacterium (formerly Propionibacterium) acnes with bone cells: A step toward understanding bone and joint infection development. *Sci. Rep.* (2017) doi:10.1038/srep42918.
78. Fischer, N. *et al.* Deciphering the intracellular fate of Propionibacterium acnes in macrophages. *Biomed Res. Int.* (2013) doi:10.1155/2013/603046.

79. Kjaer, M. *et al.* Metabolic activity and collagen turnover in human tendon in response to physical activity. *J. Musculoskelet. Neuronal Interact.* (2005).
80. Eckes, B., Wang, F., Rittié, L., Scherr, G. & Zigrino, P. Cell-populated collagen lattice models. in *Methods in Molecular Biology* vol. 1627 223–233 (Humana Press Inc., 2017).
81. Vancocin (vancomycin) dosing, indications, interactions, adverse effects, and more. <https://reference.medscape.com/drug/firvanq-vancocin-vancomycin-342573>.
82. Rybak, M. *et al.* *Therapeutic monitoring of vancomycin: A revised consensus guideline and review of the American Society of Health-System Pharmacists, the Infectious Diseases Society of America, the Pediatric Infectious Diseases Society and the Society of Infectious Diseases. American Journal of Health-System Pharmacy* vol. 22 <https://www.ashp.org/-/media/assets/policy-guidelines/docs/draft-guidelines/draft-guidelines-ASHP-IDSA-PIDS-SIDP-therapeutic-vancomycin.ashx> (2019).
83. Drott, J. B., Alexeyev, O., Bergström, P., Elgh, F. & Olsson, J. Propionibacterium acnes infection induces upregulation of inflammatory genes and cytokine secretion in prostate epithelial cells. *BMC Microbiol.* (2010) doi:10.1186/1471-2180-10-126.
84. Fassi Fehri, L. *et al.* Prevalence of Propionibacterium acnes in diseased prostates and its inflammatory and transforming activity on prostate epithelial cells. *Int. J. Med. Microbiol.* **301**, 69–78 (2011).
85. Verboogen, D. R. J., Revelo, N. H., ter Beest, M. & van den Bogaart, G. Interleukin-6 secretion is limited by self-signaling in endosomes. *J. Mol. Cell Biol.* **11**, 144–157 (2019).
86. Gabay, C. Interleukin-6 and chronic inflammation. *Arthritis Res. Ther.* **8**, S3 (2006).
87. WANG, X. & LIN, Y. Tumor necrosis factor and cancer, buddies or foes? *Acta Pharmacol. Sin.* **29**, 1275 (2008).
88. Xing, Z. *et al.* IL-6 is an antiinflammatory cytokine required for controlling local or systemic acute inflammatory responses. *J. Clin. Invest.* **101**, 311 (1998).
89. West, A. P., Koblansky, A. A. & Ghosh, S. Recognition and signaling by toll-like

- receptors. *Annual Review of Cell and Developmental Biology* (2006)
doi:10.1146/annurev.cellbio.21.122303.115827.
90. Rodenhizer, D., Cojocari, D., Wouters, B. G. & McGuigan, A. P. Development of TRACER: Tissue roll for analysis of cellular environment and response. *Biofabrication* (2016) doi:10.1088/1758-5090/8/4/045008.
 91. Xu, B. *et al.* Patterning cellular compartments within TRACER cultures using sacrificial gelatin printing. *Biofabrication* (2016) doi:10.1088/1758-5090/8/3/035018.
 92. Crane, J. K., Hohman, D. W., Nodzo, S. R. & Duquin, T. R. Antimicrobial susceptibility of *Propionibacterium acnes* isolates from shoulder surgery. *Antimicrob. Agents Chemother.* (2013) doi:10.1128/AAC.00463-13.
 93. Hatch, M. D., Daniels, S. D., Glerum, K. M. & Higgins, L. D. The cost effectiveness of vancomycin for preventing infections after shoulder arthroplasty: a break-even analysis. *J. Shoulder Elb. Surg.* (2017) doi:10.1016/j.jse.2016.07.071.
 94. Tzafetas, M. *et al.* The intelligent knife (iKnife) and its intraoperative diagnostic advantage for the treatment of cervical disease. *Proc. Natl. Acad. Sci. U. S. A.* **117**, 7338–7346 (2020).
 95. E, B. *et al.* Inflammatory blood laboratory levels as markers of prosthetic joint infection: a systematic review and meta-analysis. *J. Bone Joint Surg. Am.* **92**, 2102–2109 (2010).
 96. Platsidaki, E. & Dessinioti, C. Recent advances in understanding *Propionibacterium acnes* (*Cutibacterium acnes*) in acne. *F1000Research* **7**, (2018).
 97. Liu, P.-F., Nakatsuji, T., Zhu, W., Gallo, R. L. & Huang, C.-M. Passive immunoprotection targeting a secreted CAMP factor of *Propionibacterium acnes* as a novel immunotherapeutic for acne vulgaris. *Vaccine* **29**, 3230–3238 (2011).
 98. D, V. *et al.* Serum interleukin-6 as a marker of periprosthetic shoulder infection. *J. Bone Joint Surg. Am.* **96**, 41–45 (2014).
 99. SJ, F. *et al.* Synovial fluid interleukin-6 as a predictor of periprosthetic shoulder infection. *J. Bone Joint Surg. Am.* **97**, 63–70 (2015).
 100. Kung, M., Markantonis, J., Nelson, S. & Campbell, P. The Synovial Lining and

- Synovial Fluid Properties after Joint Arthroplasty. *Lubricants* **3**, 394–412 (2015).
101. Sophia Fox, A. J., Bedi, A. & Rodeo, S. A. The basic science of articular cartilage: Structure, composition, and function. *Sports Health* **1**, 461–468 (2009).
 102. Eleswarapu, S. V., Responde, D. J. & Athanasiou, K. A. Tensile Properties, Collagen Content, and Crosslinks in Connective Tissues of the Immature Knee Joint. *PLoS One* **6**, e26178 (2011).
 103. Tsuzaki, M., Yamauchi, M. & Banes, A. J. Tendon collagens: Extracellular matrix composition in shear stress and tensile components of flexor tendons. *Connect. Tissue Res.* **29**, 141–152 (1993).
 104. Liu JX *et al.* Topical vancomycin and its effect on survival and migration of osteoblasts, fibroblasts, and myoblasts: An in vitro study. *J. Orthop.* **15**, 53–58 (2018).
 105. Hanada, M. *et al.* Intrawound vancomycin powder increases post-operative wound complications and does not decrease periprosthetic joint infection in primary total and unicompartmental knee arthroplasties. *Knee Surgery, Sport. Traumatol. Arthrosc.* **27**, 2322–2327 (2019).
 106. Johnson, J. D. *et al.* Serum and Wound Vancomycin Levels After Intrawound Administration in Primary Total Joint Arthroplasty. *J. Arthroplasty* **32**, 924–928 (2017).
 107. Renz, N., Perka, C. & Trampuz, A. Management periprothetischer Infektionen des Kniegelenks. *Orthopade* (2016) doi:10.1007/s00132-015-3217-6.
 108. Oxoid - Product Detail.
http://www.oxid.com/UK/blue/prod_detail/prod_detail.asp?pr=CM1135&c=UK&lang=EN.
 109. Gannesen, A. V. *et al.* Composition of the biofilm matrix of cutibacterium acnes acneic strain RT5. *Front. Microbiol.* (2019) doi:10.3389/fmicb.2019.01284.
 110. Beroz, F. *et al.* Verticalization of bacterial biofilms. *Nat. Phys.* **14**, 954–960 (2018).
 111. Mayslich, C., Grange, P. A. & Dupin, N. Cutibacterium acnes as an opportunistic pathogen: An update of its virulence-associated factors. *Microorganisms* vol. 9 1–21 (2021).

112. K., T. *et al.* Classification of *Cutibacterium acnes* at phylotype level by MALDI-MS proteotyping. *Proc. Jpn. Acad. Ser. B. Phys. Biol. Sci.* (2019).
113. Vaqas, B. *et al.* SURG-31. INTRAOPERATIVE MOLECULAR DIAGNOSIS AND SURGICAL GUIDANCE USING iKNIFE REAL-TIME MASS SPECTROMETRY. *Neuro. Oncol.* (2016) doi:10.1093/neuonc/now212.831.
114. Vaqas, B., Balog, J., Roncaroli, F., Takats, Z. & O'Neill, K. Abstract LB-287: iKnife in neurosurgery: intraoperative real-time, in vivo biochemical characterization of brain tumors with high spatial resolution. in (2015). doi:10.1158/1538-7445.am2015-lb-287.
115. Alexander, J. *et al.* A novel methodology for in vivo endoscopic phenotyping of colorectal cancer based on real-time analysis of the mucosal lipidome: a prospective observational study of the iKnife. *Surg. Endosc.* (2017) doi:10.1007/s00464-016-5121-5.
116. St John, E. R. *et al.* Rapid evaporative ionisation mass spectrometry of electrosurgical vapours for the identification of breast pathology: Towards an intelligent knife for breast cancer surgery. *Breast Cancer Res.* (2017) doi:10.1186/s13058-017-0845-2.

Supplementary Information

Video S1. Step-by-step Demonstration of the Cell Seeding and S-JIM Assembly Process.

<https://www.youtube.com/watch?v=XwIru-NLM6U>

Table S1. SC Fibroblast Cellular Pathways with Enhanced Gene Expression

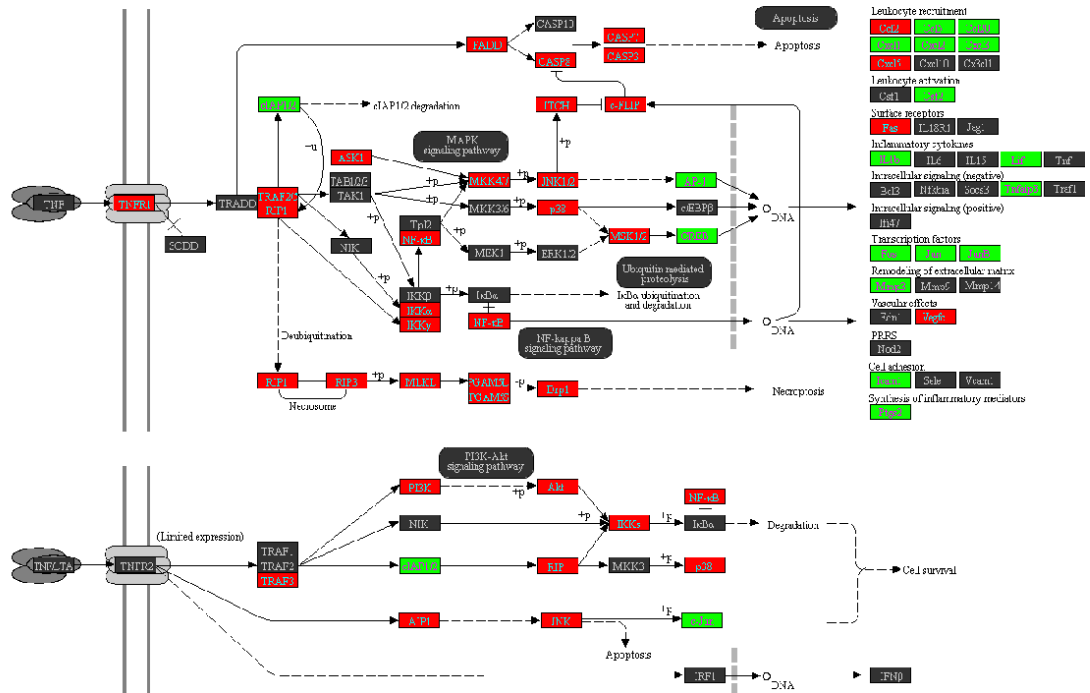
Following Co-culture with *C. acnes* in the FBCC Model. RNA libraries

were prepared from SC fibroblasts and *C. acnes* following 48 hours of co-culture and genes with a 2-fold or greater increase or reduction in expression were categorized into a list of pre-available cellular pathways using Partek Flow® data analysis software (method 2.6.6). Cellular pathways with significant changes in gene expression ($p < 0.01$) were ranked by their enrichment score (degree to which the set of genes in a pathway exhibit differential expression).

Description ↕	Enrichment score ↕	P-value ↕
Herpes simplex virus 1 infection	32.00	1.26E-14
Hepatitis B	12.89	2.53E-6
NOD-like receptor signaling pathway	12.27	4.69E-6
Measles	10.71	2.24E-5
Cell cycle	9.17	1.04E-4
Necroptosis	8.24	2.63E-4
Ubiquitin mediated proteolysis	8.23	2.66E-4
TNF signaling pathway	7.97	3.47E-4
Influenza A	7.54	5.31E-4
Spliceosome	7.54	5.31E-4
Legionellosis	6.81	1.1E-3
IL-17 signaling pathway	6.21	2E-3
Epstein-Barr virus infection	6.17	2.08E-3
Apoptosis - multiple species	5.43	4.37E-3
Antifolate resistance	5.21	5.44E-3
Apoptosis	5.08	6.2E-3
Kaposi sarcoma-associated herpesvirus infection	5.05	6.44E-3
Proteasome	5.04	6.48E-3
Platinum drug resistance	4.75	8.66E-3
Hepatitis C	4.73	8.79E-3
DNA replication	4.72	8.94E-3
Longevity regulating pathway - multiple species	4.65	9.58E-3

A

TNF SIGNALING PATHWAY



B

IL-17 SIGNALING PATHWAY

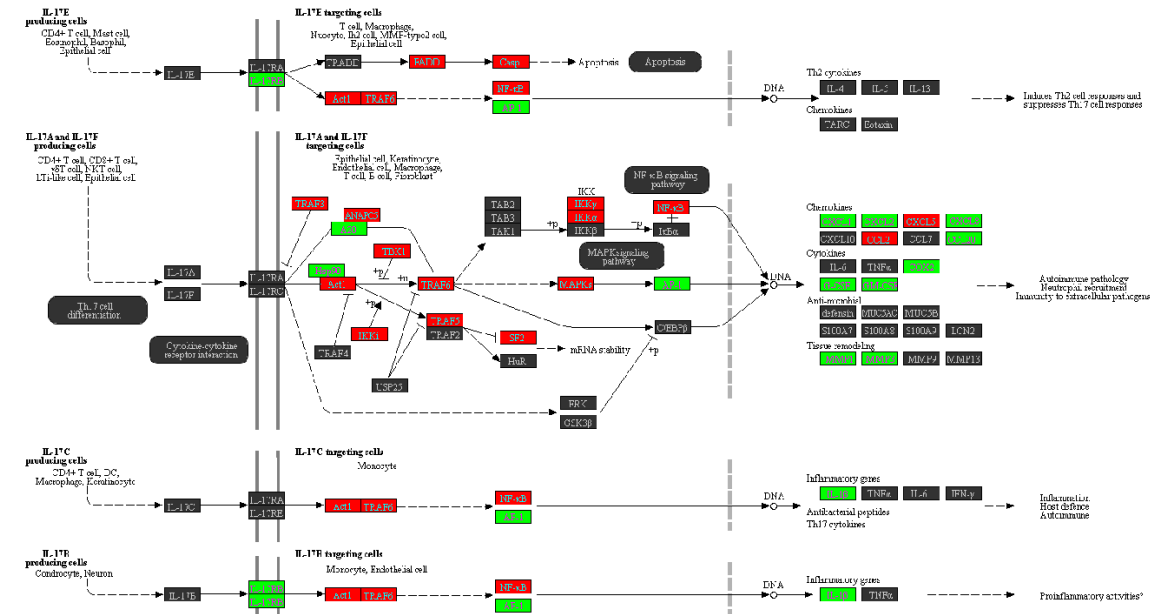


Figure S1. Differential gene expression of the (A) TNF and (B) IL-17 signaling pathways in SC fibroblasts in response to *C. acnes*.

Genes highlighted in green or red displayed significantly increased or decreased expression respectively ($p < 0.01$) by at least two-fold in response to co-culture with *C. acnes*. Early response genes (cytokines and transcription factors) and downstream transcriptional targets are separated by a thick gray dotted line.

Curriculum Vitae

Name: Tony Bohan Huang

Post-secondary Education and Degrees: Western University
London, Ontario, CA
2014-2018 BSc with Thesis in Biochemistry

Western University
London, Ontario, CA
2018-2021 MSc with Thesis in Biochemistry

Honours and Awards: Bennie and Shirley Bradshaw Award in Science
Western University
2017

Outstanding Poster Award (top 10%)
Canadian Connective Tissue Society
2019

Related Work Experiences: Summer Research Student
Institute of Medical Sciences, University of Toronto
2015

Work Study Research Student
Department of Biochemistry, Western University
2017-2018

Publications:

T.B. Huang, A.M. Pena Diaz, K.J. Faber, G.S. Athwal, M. Woolman, K. Nygard, L. Keenlside, D.B. O’Gorman (2021). Development of a 3D Bioartificial Shoulder Joint Implant Mimetic of Periprosthetic Joint Infection. Tissue Engineering Part A. Manuscript ID: TEA-2021-0081.R1

J. Miquel, **T.B. Huang**, G.S. Athwal, K.J. Faber, D.B. O’Gorman (2021). Vancomycin is Effective in Preventing *Cutibacterium acnes* Growth in a Shoulder Arthroplasty Mimetic. Journal of Shoulder and Elbow Surgery. Manuscript ID: JSES-D-21-00421R1

S.L. Brumwell, M.R. MacLeod, **T.B. Huang**, R.R. Cochrane, R.S. Meaney, M. Zamani, O. Matysiakiewicz, K.N. Dan, P. Janakirama, D.R. Edgell, T.C. Charles, T.M. Finan, B.J. Karas (2019). Designer *Sinorhizobium meliloti* Strains and Multi-functional Vectors Enable Direct Inter-kingdom DNA Transfer. PLoS ONE. Manuscript ID: PMC6576745

Select Conferences:

Orthopaedic Research Society (2020, Poster). **T.B. Huang**, A.M. Pena Diaz, K.J. Faber, G.S. Athwal, D.S. Drosdowech, D.B. O’Gorman. Development of a Pre-clinical 3D Bioartificial Human Tissue Model of Periprosthetic Joint Infections of the Shoulder.

Canadian Connective Tissue Conference (2019, Poster) **T.B. Huang**, A.M. Pena Diaz, K.J. Faber, G.S. Athwal, D.S. Drosdowech, D.B. O’Gorman. Developing an *in vitro* Model of *Cutibacterium acnes* Infection After Shoulder Surgery

London Health Research Day Conference (2019, Poster) **T.B. Huang**, A.M. Pena Diaz, K.J. Faber, G.S. Athwal, D.S. Drosdowech, D.B. O’Gorman. Development of a 3D Tissue Mimetic of Shoulder Joint Infection After Surgery.

Canadian Bone and Joint Conference (2018, Poster). **T.B. Huang**, A.M. Pena Diaz, K.J. Faber, G.S. Athwal, J. Burton, D.B. O’Gorman. Modelling Post-surgical *Cutibacterium acnes* Infections of Connective Tissue in Joints